Fluid Phase Equilibria 542–543 (2021) 113095

Contents lists available at ScienceDirect

Fluid Phase Equilibria

journal homepage: www.elsevier.com/locate/fluid

A self-consistent perturbative density functional theory for hard-core fluids: phase diagrams, structural and interfacial properties

Elvis do A. Soares[a], Amaro G. Barreto Jr.[a], Frederico W. Tavares[a,b,*]

[a] Engenharia de Processos Químicos e Bioquímicos (EPQB), Escola de Química, Universidade Federal do Rio de Janeiro, Rio de Janeiro, 21941-909, RJ, Brazil
[b] Programa de Engenharia Química (PEQ), COPPE, Universidade Federal do Rio de Janeiro, Rio de Janeiro, 21945-970, RJ, Brazil

ARTICLE INFO

Article history:
Received 27 April 2021
Revised 18 May 2021
Accepted 22 May 2021
Available online 27 May 2021

MSC:
0000
1111

Keywords:
Density functional theory
Perturbation theory
Hard-core fluids

ABSTRACT

The classical Density functional theory (DFT) has become a powerful tool to describe the microscopic structure of fluids as the radial distribution function. One of its particular capabilities is to express the thermodynamic properties of those fluids even under the influence of external potentials, such as fluid-solid interaction. However, good models for the Helmholtz free-energy functionals are necessary to improve the results. In this work, we present a self-consistent thermodynamic perturbation theory for the excess Helmholtz free-energy from the DFT applied to hard-core fluids. The new perturbation theory is solved self-consistently without any closure relation to solving the Ornstein-Zernike equation explicitly. We compare the performance of our self-consistent perturbation theory with the results obtained with the well-known second-order Barker-Henderson perturbation theory for the hard-core Yukawa and square-well fluids. Moreover, we propose two versions of the DFT to describe the perturbative contribution: one based on the weighted density approximation theory and another from a modified mean-field theory. The present results confirm the modified mean-field theory as a better option to calculate the thermodynamic and structural properties of hard-core fluids.

1. Introduction

The classical Density Functional Theory (DFT) can express the thermodynamic properties and the microscopic structure of classical fluids simultaneously. All these phenomena are described from just an excess Helmholtz free-energy model, even under the influence of external potential [1,2].

The recent formulations of the classical DFT to modeling these properties of inhomogeneous fluids are constructed from an excess Helmholtz free-energy functional written as the sum of a repulsive hard-core parcel and an attractive parcel. The repulsive contribution is well described by the modified fundamental measure theory (MFMT) [3,4]. However, the attractive contribution can be described by a density expansion [5], or a perturbation theory [6,7], or simply by a mean-field theory (MFT) approximation [8,9]. These various versions of DFT have predicted structural and interfacial properties for hard-sphere fluids [10–12], the hard-core Yukawa (YK) fluids [8,13,14], the square-well (SW) fluids [15–17], the Lennard-Jones (LJ) fluids [9], and others. Besides, there are excellent examples of successful application of DFT to confined fluids [18–25].

The MFT is computationally efficient but neglects structural correlations in the excess Helmholtz free energy functional. To correct this problem, the mainstream DFT formulations incorporate the direct correlation functions (DCF) due to the inter-particle interactions in the form of a Taylor expansion of the excess Helmholtz free-energy around a reference fluid density. Various approximate forms of DCF have been obtained from the well-known Ornstein-Zernike (OZ) equation. The OZ equation connects the direct correlation function $c^{(2)}(r)$ and the total correlation function $h(r) = g(r) + 1$, where $g(r)$ is the radial distribution function (RDF). With the help of some approximate form of the closure relation, such as the mean spherical approximation (MSA) or hypernetted chain (HNC) closures, the OZ equation can be solved analytically or numerically. For example, there are good results for the OZ solutions of SW fluids [26–28] or hard-core YK fluids [29–32].

The other attempts to DFT are based on perturbation theories of homogeneous fluids with the functional form described by a weighted density approximation (WDA) [33–35]. Undoubtedly, the best-known of these perturbation theories is the Barker-Henderson (BH) perturbation theory for attractive hard-core fluids [36–38]. Another example of perturbation theory is the thermodynamic perturbation theory (TPT) of Zhou [39] based on the numerical derivative of the RDF. This theory has the same first-order approximation, but it differs from the BH theory from the second-order term

* Corresponding author.
E-mail addresses: tavares@eq.ufrj.br, ftavares@peq.coppe.ufrj.br (F.W. Tavares).

https://doi.org/10.1016/j.fluid.2021.113095
0378-3812/

onwards. The TPT presents a second-order correction superior to a macroscopic compressibility approximation of BH [40] and can be extended until the fifth-order counterpart [41]. Indeed, the TPT needs the high derivatives of the radial distribution function obtained by some approximation of the OZ equation in the original work. However, its DFT formulation uses the MSA second-order DCF to construct the excess Helmholtz free energy density functional [41]. Both theories were applied successfully to describe SW fluids, YK fluids, and others.

The present work aims to develop a self-consistent perturbation theory from a DFT without using the OZ equation. In principle, we can use a first-order perturbative DFT to predict the radial distribution functions of the attractive potential perturbation contribution. The derivative of this RDF around the reference fluid is used to construct the second-order term for the perturbative contribution. In this way, the RDF and DCF are obtained as an output of our perturbative DFT. The approach described below can predict thermodynamic properties and the microscopic structure of hard-core YK and SW fluids. The functional form of the self-consistent perturbation theory free-energy can be build up from a modified WDA or a modified MFT. Therefore, we present the two formulations and compare their results with those of Monte-Carlo (MC) simulation and Molecular Dynamics (MD) data.

The structure of our work is as follows. In Section 2 we formulate the self-consistent perturbative density functional theory. The results of thermodynamic quantities, structural and interfacial properties are presented in Section 3. The summary and conclusions are given in Section 4.

2. Theory

2.1. The classical density functional theory

According to the DFT of classical fluids, the grand thermodynamic potential, $\Omega[\{\rho\}]$, and the Helmholtz free-energy, $F[\rho(\boldsymbol{r})]$, are functionals of the local density distribution $\rho(\boldsymbol{r})$. The grand potential functional $\Omega[\rho(\boldsymbol{r})]$ is related to the free-energy functional $F[\rho(\boldsymbol{r})]$ by a thermodynamic relation given as

$$\Omega[\rho(\boldsymbol{r})] = F[\rho(\boldsymbol{r})] + \int \mathrm{d}\boldsymbol{r}\,[V_{\mathrm{ext}}(\boldsymbol{r}) - \mu]\rho(\boldsymbol{r}) \tag{1}$$

where μ is the chemical potential and $V_{\mathrm{ext}}(\boldsymbol{r})$ is an external potential acting on the fluid. The grand potential $\Omega[\{\rho\}]$ has a minimum value when $\rho(\boldsymbol{r})$ is the equilibrium density distribution, *i.e.*, the minimum value of $\Omega[\rho(\boldsymbol{r})]$ is the equilibrium grand potential of the system. Then, the equilibrium density profile is calculated extremizing the grand canonical potential,

$$\left.\frac{\delta\Omega[\rho(\boldsymbol{r})]}{\delta\rho(\boldsymbol{r})}\right|_{\mu,T} = \frac{\delta F[\rho(\boldsymbol{r})]}{\delta\rho(\boldsymbol{r})} + V_{\mathrm{ext}}(\boldsymbol{r}) - \mu = 0. \tag{2}$$

The Helmholtz free-energy functional is determined by the sum

$$F[\rho(\boldsymbol{r})] = F_{\mathrm{id}}[\rho(\boldsymbol{r})] + F_{\mathrm{exc}}[\rho(\boldsymbol{r})], \tag{3}$$

where the first parcel is the ideal gas contribution and the second parcel is the excess free-energy parcel.

The ideal gas contribution is given analytically by the semi-classical expression

$$\beta F_{\mathrm{id}}[\rho(\boldsymbol{r})] = \int \mathrm{d}\boldsymbol{r}\,\rho(\boldsymbol{r})\big[\ln(\Lambda^3\rho(\boldsymbol{r})) - 1\big] \tag{4}$$

where $\beta = 1/k_BT$ is the inverse of the thermal energy, T is the temperature, and $\Lambda = h(\beta/2\pi m)^{1/2}$ is the de Broglie thermal wavelength with k_B, h, and m being the Boltzmann constant, the Planck constant, and the mass of the particle, respectively.

The excess free-energy functional $F_{\mathrm{exc}}[\rho(\boldsymbol{r})]$ contains all the information about the interaction between particles given by the pair potential $V(\boldsymbol{r},\boldsymbol{r}')$. This functional defines the two-body density distribution $\rho^{(2)}(\boldsymbol{r},\boldsymbol{r}')$ through the functional derivative concerning the pair potential $V(\boldsymbol{r},\boldsymbol{r}')$ in the form

$$\frac{\delta F_{\mathrm{exc}}[\rho]}{\delta V(\boldsymbol{r},\boldsymbol{r}')} = \frac{1}{2}\rho^{(2)}(\boldsymbol{r},\boldsymbol{r}'). \tag{5}$$

Because the $\rho^{(2)}(\boldsymbol{r},\boldsymbol{r}')$ is not known exactly for each pair potential $V(\boldsymbol{r},\boldsymbol{r}')$, the excess free-energy must be obtained by a thermodynamic perturbation theory. The common perturbation theory is obtained by splitting the pair potential in a hard-core repulsive parcel $v_{\mathrm{hs}}(\boldsymbol{r},\boldsymbol{r}')$ and an effective attraction parcel $\alpha u(\boldsymbol{r},\boldsymbol{r}')$, such that

$$V(\boldsymbol{r},\boldsymbol{r}',\alpha) = v_{\mathrm{hs}}(\boldsymbol{r},\boldsymbol{r}') + \alpha u(\boldsymbol{r},\boldsymbol{r}') \quad \text{for} \quad 0 \le \alpha \le 1, \tag{6}$$

where α is the coupling parameter of the pair potential. The $v_{\mathrm{hs}}(r)$ is the hard-spheres pair potential defined as

$$v_{\mathrm{hs}}(r) = \begin{cases} \infty, & r < \sigma, \\ 0, & r \ge \sigma \end{cases} \tag{7}$$

The potential defined in Eq. (6) specifies a thermodynamic path integration [42] in the form

$$F_{\mathrm{exc}}[\rho(\boldsymbol{r})] = F_{\mathrm{hs}}[\rho(\boldsymbol{r})] + F_{\mathrm{pert}}[\rho(\boldsymbol{r})], \tag{8}$$

where the first parcel represents the hard-sphere repulsive contribution and the second parcel is the perturbative contribution due to the long-range attraction.

The hard-spheres reference functional, $F_{\mathrm{hs}}[\rho(\boldsymbol{r})]$, is described by the modified fundamental measure theory (MFMT) which provides an accurate description of the fluid structures. In this work, we apply the White-Bear functional [12,43] for the hard-spheres Helmholtz free-energy contribution as

$$\beta F_{\mathrm{hs}}[\rho(\boldsymbol{r})] = \int \mathrm{d}\boldsymbol{r}\,\Phi[\{n_\xi(\boldsymbol{r})\}] \tag{9}$$

where the free-energy density function is given by

$$\Phi[\{n_\xi(\boldsymbol{r})\}] = -n_0\ln(1-n_3) + \frac{n_1n_2 - \boldsymbol{n}_{v1}\cdot\boldsymbol{n}_{v2}}{1-n_3} + \Big(n_3 + (1-n_3)^2\ln(1-n_3)\Big)\frac{n_2^3 - 3n_2\boldsymbol{n}_{v2}\cdot\boldsymbol{n}_{v2}}{36\pi n_3^2(1-n_3)^2}. \tag{10}$$

The weighted densities $n_{(\xi)}(\boldsymbol{r})$ are defined as [3]

$$n_\xi(\boldsymbol{r}) \equiv \int \mathrm{d}\boldsymbol{r}'\,\rho(\boldsymbol{r}')\omega_\xi(\boldsymbol{r}-\boldsymbol{r}') \tag{11}$$

where $\xi = 0, 1, 2, 3, v1$, and $v2$. The linearly independent weight functions are given by

$$\omega_3(\boldsymbol{r}) = \Theta(\sigma/2 - |\boldsymbol{r}|), \tag{12}$$

$$\omega_2(\boldsymbol{r}) = |\nabla\Theta(\sigma/2 - |\boldsymbol{r}|)| = \delta(\sigma/2 - |\boldsymbol{r}|), \tag{13}$$

$$\boldsymbol{\omega}_{v2}(\boldsymbol{r}) = \nabla\Theta(\sigma/2 - |\boldsymbol{r}|) = \frac{\boldsymbol{r}}{r}\delta(\sigma/2 - |\boldsymbol{r}|), \tag{14}$$

and the dependent weight functions are given by $\omega_0(\boldsymbol{r}) = \omega_2(\boldsymbol{r})/\pi\sigma^2$, $\omega_1(\boldsymbol{r}) = \omega_2(\boldsymbol{r})/2\pi\sigma$, and $\boldsymbol{\omega}_{v1}(\boldsymbol{r}) = \boldsymbol{\omega}_{v2}(\boldsymbol{r})/2\pi\sigma$. Here, $\Theta(r)$ is the Heaviside step function, and $\delta(r)$ is the Dirac delta distribution. For homogeneous fluids, the functional given by Eq. (9) simplifies to the Boublik-Mansoori-Carnahan-Starling-Leland [44] equation of state for hard-sphere mixtures, or to the Carnahan-Starling [45] for pure hard-sphere fluid is written as

$$\beta f_{\mathrm{hs}}(\rho) \equiv \beta\frac{F_{\mathrm{hs}}(\rho)}{N} = \frac{\eta(4-3\eta)}{(1-\eta)^2}, \tag{15}$$

where $\eta = (\pi/6)\rho\sigma^3$ is the packing fraction.

The perturbative functional, $F_{\text{pert}}[\rho(\boldsymbol{r})]$, can be written in the form

$$F_{\text{pert}}[\rho(\boldsymbol{r})] = \frac{1}{2}\int \mathrm{d}\boldsymbol{r}\,\rho(\boldsymbol{r})\int \mathrm{d}\boldsymbol{r}'\,\rho(\boldsymbol{r}')u(\boldsymbol{r},\boldsymbol{r}')\int_0^1 \mathrm{d}\alpha\, g(|\boldsymbol{r}-\boldsymbol{r}'|;\rho,T,\alpha). \tag{16}$$

with $g(|\boldsymbol{r}-\boldsymbol{r}'|;\rho,T,\alpha)$ being the pair-correlation function of the fluid with density ρ and temperature T. In fact, $g(r;\rho,T,\alpha=0)$ reproduce exactly the reference fluid pair correlation function, in this case, $g_{\text{hs}}(r,\rho)$. The main questions here are: how to obtain a suitable approximation for the effective pair-correlation function $g(r;\rho,T,\alpha)$ for non-zero values of α? what density value ρ must be used to calculate $g(r;\rho,T,\alpha)$? Moreover, $g(r;\rho,T,\alpha)$ must be non-analytical in most cases for the attractive potential, such that the perturbative functional has no analytical form. It is interesting to note that if $g(r;\rho,T,\alpha)\approx 1$, the perturbative functional is equivalent to the well-known mean-field theory or the structureless fluid approximation.

The perturbative contribution, $F_{\text{pert}}[\rho(\boldsymbol{r})]$, can be obtained by the following perturbation theories of homogeneous fluid. The functional is constructed using two following propose of functional form to describe inhomogeneous fluids.

2.2. The perturbation theories for homogeneous fluids

2.2.1. Barker-Henderson second-order perturbation theory

The Barker-Henderson second-order perturbation theory [36,37] is an option to describe the perturbative free-energy functional, Eq. (16), for homogeneous fluids. This perturbation can be described in terms of an effective radial pair distribution, given by

$$\int_0^1 \mathrm{d}\alpha\, g(r;\rho,T,\alpha) \approx g_{\text{hs}}(r;\rho) - \frac{1}{2}\beta u(r)\frac{\partial[\rho g_{\text{hs}}(r;\rho)]}{\partial p}. \tag{17}$$

where $g_{\text{hs}}(r;\rho)$ is the hard-sphere radial distribution function. The first parcel in Eq. (17) represents the first-order term of the perturbation theory, and the second parcel represents the second-order term on the local compressibility approximation (LCA). In the second-order theory, the local compressibility approximation provides better accuracy than the macroscopic compressibility approximation [46]. The derivative on the second-order term can be written as

$$\frac{\partial[\rho g_{\text{hs}}(r;\rho)]}{\partial p} = \kappa_{\text{hs}}(\rho)\left[g_{\text{hs}}(r;\rho) + \rho\frac{\partial g_{\text{hs}}(r;\rho)}{\partial\rho}\right], \tag{18}$$

where $\kappa_{\text{hs}}(\rho)$ is the isothermal compressibility of the hard-sphere reference fluid, which is defined as

$$\kappa_{\text{hs}}(\rho) = \left(\frac{\partial\rho}{\partial p}\right)_{\text{hs}} = \frac{(1-\eta)^4}{1+4\eta+4\eta^2-4\eta^3+\eta^4}, \tag{19}$$

obtained from the Carnahan-Starling equation of state. Consequently, the free-energy per particle of the perturbation contribution f_{pert} is written as

$$f_{\text{pert}}^{(\text{BH})}(\rho) = f_{\text{BH}}^{(1)}(\rho) + f_{\text{BH}}^{(2)}(\rho,T), \tag{20}$$

with

$$f_{\text{BH}}^{(1)}(\rho) = 2\pi\rho\int_0^\infty \mathrm{d}r\, r^2 u(r) g_{\text{hs}}(r;\rho), \tag{21}$$

$$f_{\text{BH}}^{(2)}(\rho,T) = -\pi\beta\rho\kappa_{\text{hs}}(\rho)\frac{\partial}{\partial\rho}\left[\rho\int_0^\infty \mathrm{d}r\, r^2[u(r)]^2 g_{\text{hs}}(r;\rho)\right]. \tag{22}$$

The hard-sphere pair correlation is calculated following the procedure discussed in Section 3.3. We construct a grid of density range of $\rho\sigma^3\in[0.0,1.0]$ with the step of 0.02 and radial coordinate range of $r/\sigma\in[1.0,5.0]$ with a step of 0.01. With this, the two terms of the BH perturbation theory, Eqs. (21) and (22), are interpolated with a cubic Hermite spline and a bi-cubic Hermite spline, respectively. For more details about the interpolation, see Appendix C.

2.2.2. Self-consistent perturbation theory

The self-consistent perturbation theory (SCPT) is presented here as another option to describe the perturbative free-energy, Eq. (16), for homogeneous fluids. This theory is obtained by combining the radial distribution function calculated using the DFT with a thermodynamic perturbation theory. The starting point is the thermodynamic perturbation theory known as coupling parameter series expansion [39,47]. This perturbation theory is based on writing the radial distribution function integral, Eq. (16), with the Taylor series by

$$\int_0^1 g(r;\rho,T,\alpha)\mathrm{d}\alpha = \frac{1}{n!}\sum_{n=0}^\infty \int_0^1 \alpha^n \frac{\partial^n g(r;\rho,T,\alpha)}{\partial\alpha^n}\Big|_{\alpha=0}\mathrm{d}\alpha\,, \tag{23}$$

where α is the coupling parameter, and the thermodynamic derivatives are taken around the reference fluid. Using this expansion to solve the perturbative integral Eq. (16) and retaining only the two first terms of that expansion, we get

$$f_{\text{pert}}^{(\text{SCPT})}(\rho,T) = f_{\text{SCPT}}^{(1)}(\rho) + f_{\text{SCPT}}^{(2)}(\rho,T), \tag{24}$$

with

$$f_{\text{SCPT}}^{(1)}(\rho) = 2\pi\rho\int_0^\infty \mathrm{d}r\, r^2 u(r) g_{\text{hs}}(r;\rho), \tag{25}$$

$$f_{\text{SCPT}}^{(2)}(\rho,T) = \pi\rho\int_0^\infty \mathrm{d}r\, r^2 u(r)\frac{\partial g(r;\rho,T,\alpha)}{\partial\alpha}\bigg|_{\alpha=0}, \tag{26}$$

where the first term of this perturbation theory is exactly the first term on the BH perturbation theory, Eq. (21). The *self-consistency* of our theory is obtained by calculating the derivative of the radial distribution function $\partial g(r;\rho,T,\alpha)/\partial\alpha|_{\alpha=0}$ from the DFT.

As well as in the BH perturbation theory, the two terms of the SCPT perturbation theory, Eq. (25) and Eq. (26), are interpolated with a cubic Hermite spline and a bi-cubic Hermite spline, respectively. For more details, see Appendix C.

2.3. The DFT description of perturbative contribution for inhomogeneous fluids

2.3.1. The modified weighted density approximation

The modified weighted density approximation (MWDA) [33,35,48] of the excess free-energy function is written as

$$F_{\text{exc}}[\rho(\boldsymbol{r})] = F_{\text{hs}}[\rho(\boldsymbol{r})] + F_{\text{wda}}[\rho(\boldsymbol{r})], \tag{27}$$

with just the perturbation contribution being written in the WDA formalism. The basic idea of the WDA formalism is to make a free-energy of homogeneous fluid valid in the functional form, applicable to inhomogeneous systems. In this form, the perturbation free-energy can be written as

$$F_{\text{wda}}[\rho(\boldsymbol{r})] = \int \mathrm{d}\boldsymbol{r}\,\overline{\rho}(\boldsymbol{r}) f_{\text{pert}}(\overline{\rho}(\boldsymbol{r}),T), \tag{28}$$

where $f_{\text{pert}}(\overline{\rho}(\boldsymbol{r}),T)$ is the perturbative contribution of the excess free-energy per particle for a uniform fluid with density $\overline{\rho}(\boldsymbol{r})$ and temperature T. The weighted density $\overline{\rho}(\boldsymbol{r})$ is defined as

$$\overline{\rho}(\boldsymbol{r}) = \int \mathrm{d}\boldsymbol{r}'\,\rho(\boldsymbol{r}')\omega(\boldsymbol{r}-\boldsymbol{r}'), \tag{29}$$

and the normalized weight function [49] given by

$$\omega(r) = \frac{3}{4\pi\psi^3\sigma^3}\Theta(\psi\sigma - r), \tag{30}$$

Table 1
The integral of the potential $u(r)$ and the size parameter ψ for the MWDA implementation of different potentials.

Parameter	Yukawa (YK)	Square Well (SW)
a[a]	$-\frac{4}{3}\pi\epsilon\sigma^3\left(\frac{3(1+\lambda\sigma)}{(\lambda\sigma)^2}+1\right)$	$-\frac{4}{3}\pi\epsilon\sigma^3\lambda^3$
ψ	$\left(\frac{3(1+\lambda\sigma)}{(\lambda\sigma)^2}+1\right)^{1/3}$	λ

[a] The potential integral is $a=\int_0^\infty \mathrm{d}r\, 4\pi r^2 u(r)$.

where the parameter ψ scales the size of the averaging space. In this work, we define the size parameter ψ by the relation

$$\psi=\left[-\frac{3}{4\pi\epsilon\sigma^3}\int_0^\infty \mathrm{d}r\, 4\pi r^2 u(r)\right]^{1/3}, \tag{31}$$

which scales with the WCA energy volume of the perturbative potential. Here, ϵ is the energy scale of the perturbative potential, as shown in Table 1 for the YK and SW potentials. This definition of the ψ is different from the usual implementations of the WDA, but already used in DFT versions as the PC-SAFT used to describe Lennard-Jones inhomogeneous fluids [22].

From this functional form, the first-order direct correlation function (DCF) is given by

$$c^{(1)}_{\mathrm{exc}}(\boldsymbol{r},[\rho])=-\beta\frac{\delta F_{\mathrm{exc}}[\rho(\boldsymbol{r})]}{\delta\rho(\boldsymbol{r})}=c^{(1)}_{\mathrm{hs}}(\boldsymbol{r}) - \beta\int \mathrm{d}\boldsymbol{r}'\,\frac{\partial[\overline{\rho}(\boldsymbol{r}')f_{\mathrm{pert}}(\overline{\rho}(\boldsymbol{r}'))]}{\partial\overline{\rho}(\boldsymbol{r}')}\omega(\boldsymbol{r}-\boldsymbol{r}'), \tag{32}$$

and the second-order DCF in the form

$$\begin{aligned} c^{(2)}_{\mathrm{exc}}\left(\boldsymbol{r}-\boldsymbol{r}',[\rho]\right)&=-\beta\tfrac{\partial^2 F_{\mathrm{exc}}[\rho(\boldsymbol{r})]}{\partial\rho(\boldsymbol{r})\partial\rho(\boldsymbol{r}')}=c^{(2)}_{\mathrm{hs}}\left(\boldsymbol{r}-\boldsymbol{r}'\right)\\ -\beta\int \mathrm{d}\boldsymbol{r}''\,\tfrac{\partial^2[\overline{\rho}(\boldsymbol{r}'')f_{\mathrm{pert}}(\overline{\rho}(\boldsymbol{r}''))]}{\partial\overline{\rho}(\boldsymbol{r}'')^2}&\omega\left(\boldsymbol{r}'-\boldsymbol{r}''\right)\omega\left(\boldsymbol{r}-\boldsymbol{r}''\right), \end{aligned} \tag{33}$$

i.e., the pair direct correlation function is the sum of the second-order DCF inhomogeneous hard-sphere reference fluid and a term proportional to non-local perturbative compressibility. In the limit of a homogeneous fluid, the Eq. (33) reduces to

$$\begin{aligned} c^{(2)}_{\mathrm{exc}}(r,\rho_b)&=c^{(2)}_{\mathrm{hs}}(r)\\ -\beta\tfrac{\partial^2(\rho_b f_{\mathrm{pert}})}{\partial\rho_b^2}\tfrac{3}{\pi}&\left(r^3-3r(2\psi\sigma)^2+2(2\psi\sigma)^3\right)\Theta(2\psi\sigma-r). \end{aligned} \tag{34}$$

This DCF gives the correct short-ranged correlations arising from the repulsive interaction, but it does not provide the correct form of the asymptotic tail correction of the correlations for any temperature.

2.3.2. The modified mean-field theory

The modified mean-field approach (MMFT) consists of a mean-field functional in addition to a correction term due to the correlation with the hard-core region. Therefore, the excess free-energy functional is written as

$$F_{\mathrm{exc}}[\rho(\boldsymbol{r})]=F_{\mathrm{hs}}[\rho(\boldsymbol{r})]+F_{\mathrm{mft}}[\rho(\boldsymbol{r})]+F_{\mathrm{corr}}[\rho(\boldsymbol{r})], \tag{35}$$

where the mean-field theory term is

$$F_{\mathrm{mft}}[\rho(\boldsymbol{r})]=\frac{1}{2}\int \mathrm{d}\boldsymbol{r}\,\rho(\boldsymbol{r})\int \mathrm{d}\boldsymbol{r}'\,\rho(\boldsymbol{r}')u(|\boldsymbol{r}-\boldsymbol{r}'|), \tag{36}$$

and F_{corr} is the correction term. This correction term is necessary to represent the correlation between the short-range repulsive interactions and the long-range interactions. In this work, the Helmholtz free-energy functional of the correlation effects is written with the WDA formalism as

$$F_{\mathrm{corr}}[\rho(\boldsymbol{r})]=\int \mathrm{d}\boldsymbol{r}\,\overline{\rho}(\boldsymbol{r})f_{\mathrm{corr}}(\overline{\rho}(\boldsymbol{r}),T), \tag{37}$$

with the weighted density $\overline{\rho}(\boldsymbol{r})$ defined by Eq. (29) and the normalized weight function given by Eq. (30) but now with the fixed value of $\psi=0.5$. This functional form was motivated by the work of Yu [50].

The correlation parcel of the Helmholtz free-energy per particle is

$$f_{\mathrm{corr}}(\rho,T)=f^{(1)}_{\mathrm{pert}}(\rho)+f^{(2)}_{\mathrm{pert}}(\rho,T)-\frac{1}{2}\rho a, \tag{38}$$

where the last parcel represents the mean-field theory term with a being the integral of the potential $u(r)$, as shown in Table 1.

From this MMFT functional form, the first-order direct correlation function (DCF) is given by

$$\begin{aligned} c^{(1)}_{\mathrm{exc}}(\boldsymbol{r},[\rho])&=-\beta\frac{\delta F_{\mathrm{exc}}[\rho(\boldsymbol{r})]}{\delta\rho(\boldsymbol{r})}\\ &=c^{(1)}_{\mathrm{hs}}(\boldsymbol{r},[\rho])-\beta\int \mathrm{d}\boldsymbol{r}'\,\rho(\boldsymbol{r}')u(|\boldsymbol{r}-\boldsymbol{r}'|)\\ &-\beta\int \mathrm{d}\boldsymbol{r}'\,\frac{\partial[\overline{\rho}(\boldsymbol{r}'')f_{\mathrm{corr}}(\overline{\rho}(\boldsymbol{r}''))]}{\partial\overline{\rho}(\boldsymbol{r}'')}\omega_{\mathrm{corr}}(\boldsymbol{r}-\boldsymbol{r}'), \end{aligned} \tag{39}$$

and the second-order DCF in the form

$$\begin{aligned} c^{(2)}_{\mathrm{exc}}\left(\boldsymbol{r}-\boldsymbol{r}',[\rho]\right)&=-\beta\tfrac{\delta^2 F_{\mathrm{exc}}[\rho(\boldsymbol{r})]}{\delta\rho(\boldsymbol{r})\delta\rho(\boldsymbol{r}')}\\ &=c^{(2)}_{\mathrm{hs}}\left(\boldsymbol{r}-\boldsymbol{r}',[\rho]\right)-\beta u(|\boldsymbol{r}-\boldsymbol{r}'|)\\ -\beta\int \mathrm{d}\boldsymbol{r}''\,\tfrac{\partial^2[\overline{\rho}(\boldsymbol{r}'')f_{\mathrm{corr}}(\overline{\rho}(\boldsymbol{r}''))]}{\partial\overline{\rho}(\boldsymbol{r}'')^2}&\omega_{\mathrm{corr}}\left(\boldsymbol{r}'-\boldsymbol{r}''\right)\omega_{\mathrm{corr}}\left(\boldsymbol{r}-\boldsymbol{r}''\right), \end{aligned} \tag{40}$$

i.e., the pair direct correlation function is the sum of the second-order DCF inhomogeneous hard-sphere reference fluid, a term proportional to the attractive pair potential and the last term proportional to the non-local correction of the compressibility. In the limit of a homogeneous fluid, the Eq. (40) reduces to

$$\begin{aligned} c^{(2)}_{\mathrm{exc}}(r,\rho_b)&=c^{(2)}_{\mathrm{hs}}(r,\rho_b)-\beta u(r)\\ -\beta\tfrac{\partial^2[\rho_b f_{\mathrm{corr}}(\rho_b,T)]}{\partial\rho_b^2}\tfrac{3}{\pi}&\left(r^3-3r\sigma^2+2\sigma^3\right)\Theta(\sigma-r). \end{aligned} \tag{41}$$

This DCF gives the short-ranged correlations arising from repulsive forces between the particles and the correct asymptotic tail correction of the correlations on low-temperature limit i.e., $c^{(2)}\approx-\beta u(r)$ as $r\to\infty$. This result is a combination, at some point, of the two low-density tail corrections presented by Lutsko in Ref. [51].

2.4. The self-consistent algorithm

The *self-consistent* procedure of our thermodinamic perturbation theory, SCPT, for both DFT approaches, is implemented following the steps:

1. Calculate the $f^{(1)}_{\mathrm{SCPT}}(\rho)$ using the hard-sphere radial distribution function $g_{\mathrm{hs}}(r;\rho)$ and for each effective potential $\alpha u(r)$ with $\alpha=[-0.2,-0.1,0.1,0.2]$;
2. Construct the functional $F_{\mathrm{pert}}[\rho(\boldsymbol{r})]$ with just the first-order perturbation term $f^{(1)}_{\mathrm{SCPT}}(\rho)$;
3. Using the excess free-energy $F_{\mathrm{exc}}[\rho(\boldsymbol{r})]=F_{\mathrm{hs}}[\rho(\boldsymbol{r})]+F_{\mathrm{pert}}[\rho(\boldsymbol{r})]$, calculate the radial distribution function $g_{\mathrm{hs}}(r;\rho,T,\alpha)$ for each previous α values;
4. Calculate the $f^{(2)}_{\mathrm{SCPT}}(\rho)$ using the the numerical derivative of the radial distribution function$\partial g(r;\rho,T,\alpha)/\partial\alpha\,\big|_{\alpha=0}$;
5. Construct the functional $F_{\mathrm{pert}}[\rho(\boldsymbol{r})]$ with the two terms of the perturbation theory for the original potential $u(r)$;

The derivative $\partial g(r;\rho,T,\alpha)/\partial\alpha\,\big|_{\alpha=0}$ necessary to calculate the Eq. (26) is obtained by a fourth-order of accuracy central finite differences method on α, in the form

$$\begin{aligned} \left.\frac{\partial g(r;\rho,T,\alpha)}{\partial\alpha}\right|_{\alpha=0}&=\frac{g(r;\rho,T,-2\Delta\alpha)-8g(r;\rho,T,-\Delta\alpha)}{12\Delta\alpha}\\ &+\frac{8g(r;\rho,T,\Delta\alpha)-g(r;\rho,T,2\Delta\alpha)}{12\Delta\alpha} \end{aligned} \tag{42}$$

with the step value $\Delta\alpha=0.1$. This step value is discussed in Ref. [52] and it seems to be suitable only for lower derivatives.

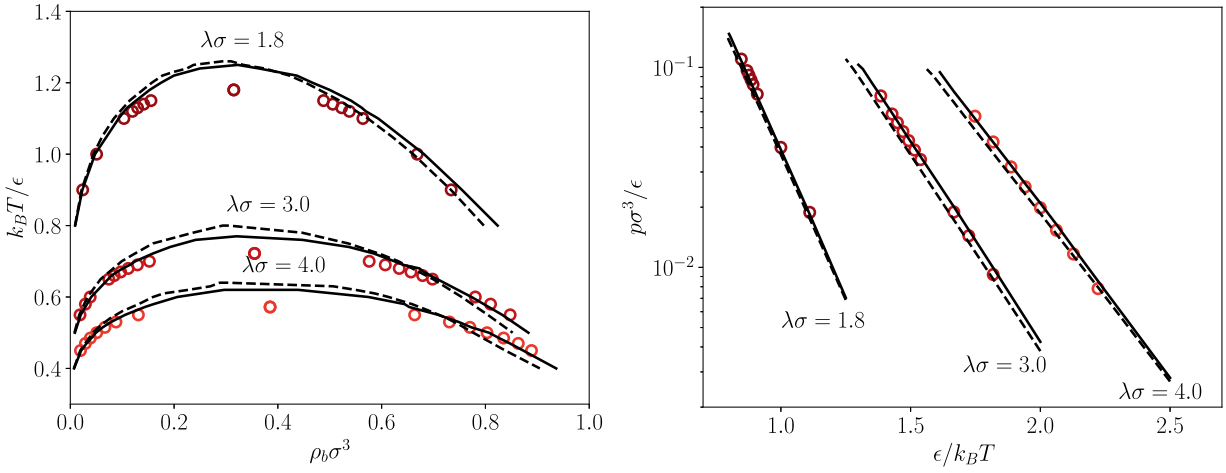

Fig. 1. (a) Phase diagrams in the $\rho - T$ plane and (b) the saturation pressures of attractive hard-core Yukawa fluids with range $\lambda\sigma = 1.8,\ 3.0,\ 4.0$ and 8.0. Open symbols: MC data from Ref. [59]. Dashed line: 2-order BH. Solid line: our SCPT.

3. Results and Discussion

We apply both perturbation theories to two cases of the attractive potential $u(r)$. The Yukawa (YK) potential is represented by

$$u(r) = \begin{cases} -\epsilon, & r < \sigma, \\ -\epsilon \frac{e^{-\lambda(r-\sigma)}}{r/\sigma}, & r \geq \sigma \end{cases} \tag{43}$$

and the Square-Well (SW) potential is given by

$$u(r) = \begin{cases} -\epsilon, & r < \sigma, \\ -\epsilon, & \sigma \leq r < \lambda\sigma, \\ 0, & r \geq \lambda\sigma \end{cases} \tag{44}$$

where ϵ is the energy scale and λ is a range parameter for each potential. The hard-core values of both $u(r)$ do not matter for the perturbation theories, but they are relevant to the MMFT implementation.

In addition to the two perturbation theories, SCPT and BH, we have two varieties of DFT implementations, MWDA and MMFT. Totalizing 4 different DFT models to validate. To quantitatively evaluate the goodness of each presented model, we use the likelihood [53] $\mathcal{L}$ defined in the form

$$\mathcal{L} = e^{-\chi^2/2} \quad \text{and} \quad \chi^2 = \sum_i \frac{(y_i - f(x_i))^2}{(y_{\max} - y_{\min})^2}, \tag{45}$$

with χ^2 being the normalized residual sum of squares [54], $\{x_i, y_i\}$ representing the MC data and $f(x_i)$ being the predicted value at x_i by the model. The normalization factor $1/(y_{\max} - y_{\min})^2$ defines a scale of the MC data because we do not have access to the MC data dispersion. With this normalization we can compare χ^2 for different types of MC data, as density, pressure and radial distribution function. The total goodness of the model is defined as the sum of the goodness of each curve described by the model, $\chi^2_{\text{total}} = \sum_n \chi^2_n$. The closer to 1 is $\mathcal{L}$, the better the model. Hence, the likelihood $\mathcal{L}$ value should only be compared between different models.

3.1. Fluid Phase Diagram and Thermodynamic quantities

For the bulk homogeneous fluid phase, the grand potential per volume can be calculated as a simple function of the bulk density ρ_b in the form

$$\frac{\Omega}{V} = k_BT\Big[\ln(\rho_b\Lambda^3) - 1\Big]\rho_b + f_{\text{hs}}(\rho_b)\rho_b + f_{\text{pert}}(\rho_b)\rho_b - \mu\rho_b, \tag{46}$$

where Eq. (15) gives the hard-sphere contribution, and the perturbation contribution is given by Eqs. (20) or (24). In such a manner, the equilibrium condition, Eq. (2), is reduced to

$$\left.\frac{\partial(\Omega/V)}{\partial\rho_b}\right|_{\mu,T} = k_BT\ln(\rho_b\Lambda^3) + \frac{\partial(\rho_b f_{\text{hs}})}{\partial\rho_b} + \frac{\partial(\rho_b f_{\text{pert}})}{\partial\rho_b} - \mu = 0, \tag{47}$$

which is the thermodynamic relation between the free-energy derivative and the chemical potential. The coexistence between the vapor and liquid phases is determined by the two densities ρ_v and ρ_l, which satisfies the Eq. (47) and the relation $[\Omega/V]_v = [\Omega/V]_l$ for the same chemical potential μ. In fact, this two relations reproduce the phase equilibria condition of

$$\mu_v = \mu_l \quad \text{and} \quad p_v = p_l. \tag{48}$$

The last condition in Eq. (48) is readily demonstrated by definition $\Omega/V = -p$ for a homogeneous fluid. Finally, the equilibrium condition is solved using a fast inertial relaxation engine (FIRE) [55,56] implemented in Python by our group [57] and discussed in a submitted paper [58]. The algorithm convergence criterion is $|\partial(\Omega/V)/\partial\rho_b| \leq \texttt{atol} = 10^{-7}$.

For the hard-core YK fluid, Fig. 1 presents the vapor-liquid coexistence curves and the saturation pressures obtained with the BH perturbation theory and SCPT for $\lambda\sigma = 1.8$, 3.0, and 4.0. The SCPT predicts the liquid coexistence density with excellent performance when compared with the Monte Carlo (MC) simulation data from Ref. [59]. The improvement in the likelihood to describe the MC data is statistically insignificant. However, the saturation pressures are better predicted by the SCPT, when compared to the BH perturbation theory, an improvement of almost 3% on the likelihood to represent the MC data, as shown in Table 2.

For the SW fluid, Fig. 2 presents the vapor-liquid coexistence curves and the saturation pressures obtained with the BH perturbation theory and SCPT for $\lambda\sigma = 1.5$, 1.75, and 2.0. The SCPT predicts the liquid coexistence line and the saturation pressure better than the BH perturbation theory when compared to the MC data from Ref. [60]. The total likelihood of SCPT to describe the MC data presents an increase of almost 10% in relation to the BH total likelihood, as shown in Table 2.

Therefore, these results of the thermodynamic properties declare our second-order SCPT as a significant improvement on the data prediction when compared to the second-order BH theory.

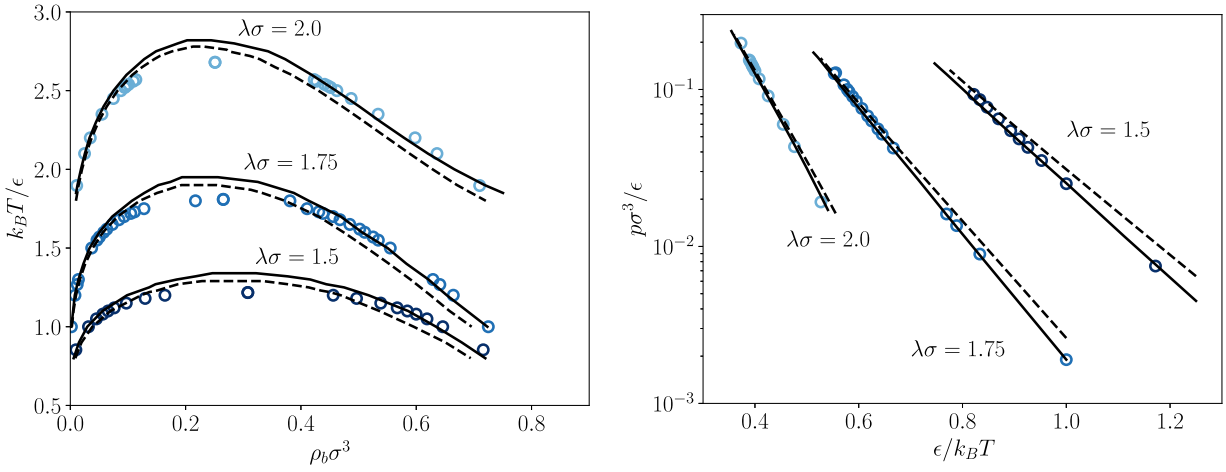

Fig. 2. (a) Phase diagrams in the $\rho - T$ plane and (b) the saturation pressures of attractive hard-core square-well fluids with range $\lambda\sigma = 1.5,\ 1.75$ and 2.0. Open symbols: MC data from Ref. [60]. Dashed line: 2-order BH. Solid line: our SCPT.

Table 2
The likelihood $\mathcal{L}$ of each perturbation theory for the different potentials to represent the MC/MD simulation data of liquid-coexistence density ρ_l and logarithm of the saturation pressure $\log_{10} p_{\text{sat}}$.

Potential	Perturbation	ρ_l	$\log_{10} p_{\text{sat}}$	Total[a]
YK	BH	67%	96%	64%
	SCPT	68%	99.4%	68%
SW	BH	90%	98%	88%
	SCPT	97%	99.6%	97%

[a] The total likelihood is the product $\mathcal{L}_{\text{total}} = \mathcal{L}_{\rho_l}\mathcal{L}_{\log_{10} p_{\text{sat}}}$.

3.2. Density profiles near a Wall

The grand potential, Eq. (1) in a planar geometry, must be obtained using the 1D planar convolutions, described in Appendix A and Appendix B. The equilibrium condition, Eq. (2), is reduced to

$$\frac{\delta\Omega[\{\rho(z)\}]}{\delta\rho(z)} = k_BT\ln[\rho(z)\Lambda^3] - \beta c^{(1)}_{\text{hs}}(z) - \beta c^{(1)}_{\text{pert}}(z) + V_{\text{ext}}(z) - \mu = 0. \tag{49}$$

Again, the equilibrium condition, Eq. (49), is achieved by minimizing of the grand potential using the FIRE algorithm. The initial density profile is set as uniform with value ρ_b. The planar geometry is spatially discretized with a grid spacing of 0.01σ and length $L = 5\sigma$, or defined H in slit-pores. The algorithm convergence criterion is $\max\{|\delta\Omega[\{\rho\}]/\delta\rho(z)|\} \le \texttt{atol} = 10^{-7}$.

For the YK fluid, and to compare with the MC simulation data available in the literature, we use the exponential external potential for the YK fluid given in the form

$$V_{\text{ext}}(z) = \begin{cases} \infty, & z < \sigma/2, \\ -\epsilon_w \exp(-\lambda(z-\sigma/2)), & z > \sigma/2, \end{cases} \tag{50}$$

where ϵ_w is the energy parameter of the wall.

The Figs. 3 and 4 present our DFT results of density profiles $\rho(z)$ for an attractive YK fluid near an attractive hard-wall in comparison with the MC simulation data [8] for $\rho_b\sigma^3 = 0.7$ and $\rho_b\sigma^3 = 0.4$, respectively, and different values of the wall attraction intensity parameter ϵ_w. In most cases, all the DFT formulations considered provide very good accuracy and are practically indistinguishable at the scales of the figures. Except for the case with $\rho_b\sigma^3 = 0.7$ and $\epsilon_w/\epsilon = 0$ where the MMFT-SCPT seems to be the most appropriate DFT formulation to represent the MC data. In fact, the density profile predicted by the MMFT-SCPT is very close to the MC data and the density of the fluid on the wall has its best value with this model. As shown in Table 3, the MMFT-SCPT represents an increase of 51% in likelihood when compared to the MMFT-BH formulation.

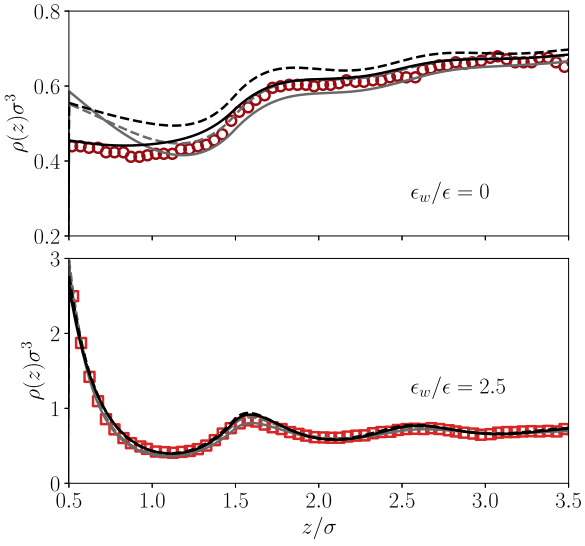

Fig. 3. Density profiles for an attractive Yukawa fluid with $\lambda\sigma = 1.8$ near a Yukawa wall at reduced temperature $k_BT/\epsilon = 1.1$ and reduced density $\rho_b\sigma^3 = 0.7$ with two different values of ϵ_w. Open symbols: MC data from Ref. [8]. Dashed grey line: MWDA-BH. Solid grey line: MWDA-SCPT. Dashed black line: MMFT-BH. Solid black line: MMFT-SCPT.

For the attractive SW fluid, Fig. 5 presents the DFT results obtained for the density profile $\rho(z)$ inside a slit-pore and the MC simulation data available in the literature [61] for $\lambda\sigma = 1.5$ and two values of density and size of the pore, H. The MMFT-SCPT formulation represents the MC data very well, mostly very close to the wall. In essence, this improvement was possible due to the better description of the fluid pressure because $\lim_{z\to 0^+}\rho(z) = \beta P$.

The attractive hard-wall for the SW fluid is simulated with the external potential defined by

$$V_{\text{ext}}(z) = \begin{cases} \infty, & z < \sigma/2, \\ -\epsilon_w, & \sigma/2 < z < \lambda\sigma - \sigma/2, \\ 0, & z > \lambda\sigma - \sigma/2 \end{cases} \tag{51}$$

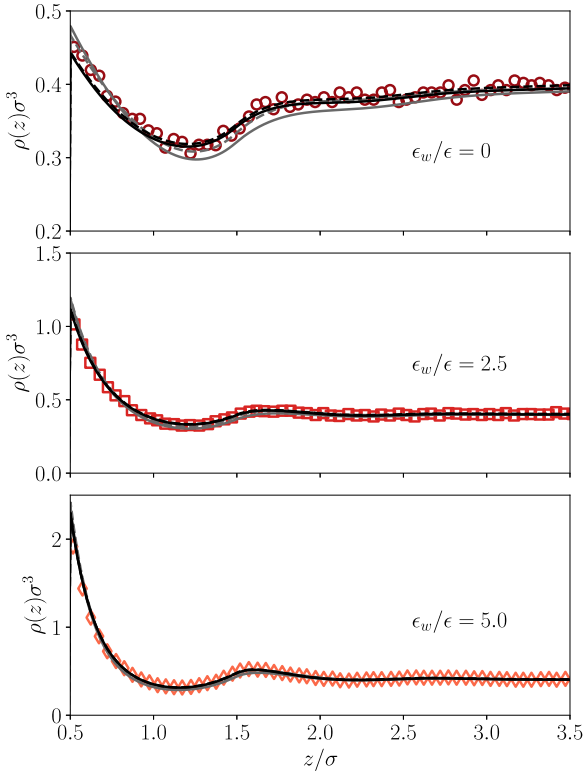

Fig. 4. Density profiles for an attractive Yukawa fluid with $\lambda\sigma = 1.8$ near a Yukawa wall at reduced temperature $k_BT/\epsilon = 2.0$ and reduced density $\rho_b\sigma^3 = 0.4$ with two different values of ϵ_w. Open symbols: MC data [8]. Dashed grey line: MWDA-BH. Solid grey line: MWDA-SCPT. Dashed black line: MMFT-BH. Solid black line: MMFT-SCPT.

Table 3
The likelihood $\mathcal{L}$ of each DFT approach for the different potentials to represent the MC/MD simulation data of density profile near a wall $\rho(z)$, radial distribution function $g(r)$ and interfacial tension γ.

Potential	Model	$\rho(z)$	$g(r)$	γ	Total[a]
YK	MWDA-BH	52%	40%	62%	13%
	MMFT-BH	22%	39%	73%	6%
	MWDA-SCPT	36%	40%	67%	10%
	MMFT-SCPT	73%	39%	69%	20%
SW	MWDA-BH	3%	95%	57%	1.6%
	MMFT-BH	14%	93%	82%	11%
	MWDA-SCPT	21%	96%	6%	1.2%
	MMFT-SCPT	57%	92%	93%	49%

[a] The total likelihood is the product $\mathcal{L}_{\text{total}} = \mathcal{L}_{\rho(z)}\mathcal{L}_{g(r)}\mathcal{L}_{\gamma}$.

where ϵ_w is the wall interaction intensity and λ is the interaction range parameter. In Fig. 6, the MC simulation data from Ref. [15] represented by the open symbols were obtained using the NVT ensemble. Our DFT results are obtained such that the mean density value $\bar{\rho}\sigma^3$ be the same as the MC data. Once more, the MMFT-SCPT predicts the density profile with a quite good performance, mainly in the attraction region of the wall. The density profiles for $\bar{\rho}\sigma^3 = 0.730$ predicted with both DFT formulations present a little deviation from the MC data. One possible explanation is the proximity of the triple point and our lack to describe a solid phase in this work. Lastly, these results represent an increase of 36% in the likelihood of MMFT-SCPT describing the MC data compared to the MWDA-SCPT results, as shown in Table 3.

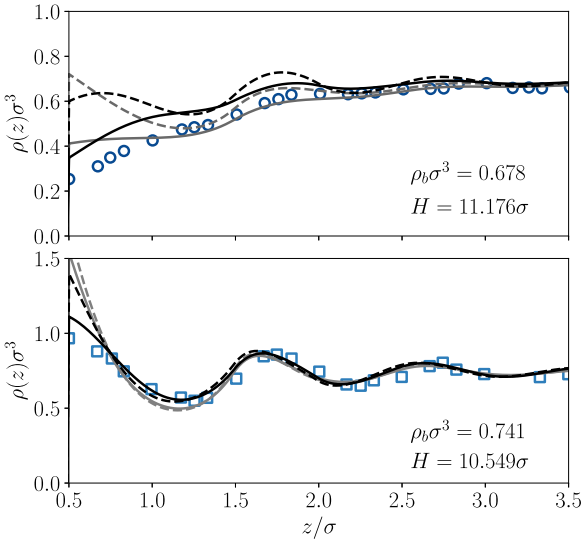

Fig. 5. Density profiles for an attractive square-well fluid with $\lambda\sigma = 1.5$ inside a hard slit-like pore of length H at temperature $k_BT/\epsilon = 1.0$ and two different mean densities $\overline{\rho}\sigma^3$. Open symbols: MC data [61]. Dashed grey line: MWDA-BH. Solid grey line: MWDA-SCPT. Dashed black line: MMFT-BH. Solid black line: MMFT-SCPT.

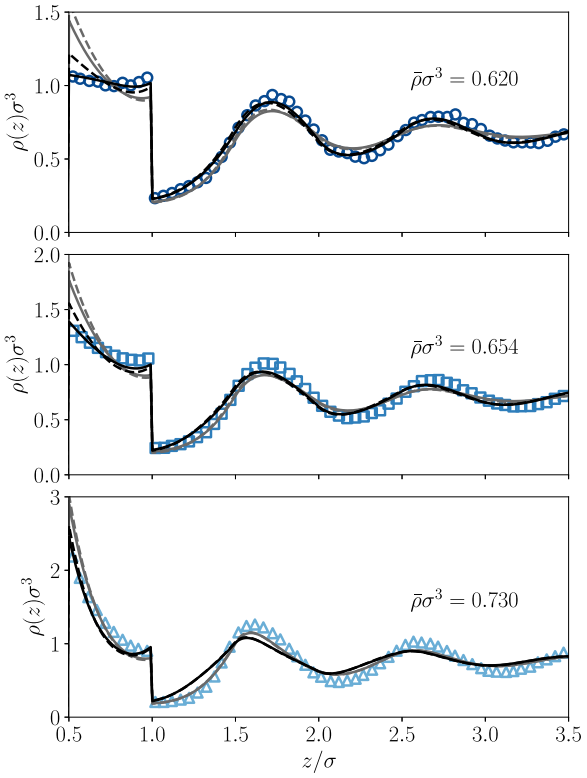

Fig. 6. Density profiles for an attractive square-well fluid with $\lambda\sigma = 1.5$ confined in an attractive square-well pore at reduced temperature $k_BT/\epsilon = 1.0$ and three different mean reduced densities $\overline{\rho}\sigma^3$. The pore size is $H = 10\sigma$ and the wall attraction parameter is $\epsilon_w = 1.5$. Open symbols: MC data [15]. Dashed grey line: MWDA-BH. Solid grey line: MWDA-SCPT. Dashed black line: MMFT-BH. Solid black line: MMFT-SCPT.

3.3. Radial Distribution Function

The radial distribution function $g(r)$ can be calculated using the Percus' test-particle method. The idea of this method is that the system is invariant when a particle is fixed at the origin; the pair correlation functions are equivalent to the reduced density profiles

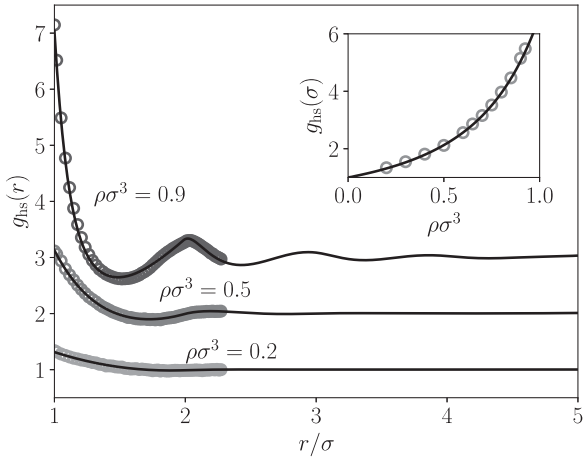

Fig. 7. Radial distribution function for the reference fluid of hard spheres. The *inset* presents the contact value of the radial distribution as a function of the density $\rho\sigma^3$. Open symbols: MC data from Ref. [62]. Solid black line: FMT. The distributions of $\rho\sigma^3 = 0.5$ and $\rho\sigma^3 = 0.9$ are shifted upward by 1.0 and 2.0.

of other species around the fixed particle. As the grand potential $\Omega[\rho(\boldsymbol{r})]$ reaches a minimum at equilibrium, the radial distribution function $g(\boldsymbol{r})$ satisfies the Euler-Lagrange equation

$$\frac{\delta\Omega[\rho(\boldsymbol{r})]}{\delta\rho(\boldsymbol{r})} = k_B T \ln\left[\frac{\rho(\boldsymbol{r})}{\rho_b}\right] - k_B T c^{(1)}_{\text{exc}}(\boldsymbol{r},[\rho]) + V_{\text{ext}}(\boldsymbol{r}) - \mu_{\text{exc}} = 0, \tag{52}$$

with the excess chemical potential $\mu_{\text{exc}} = \mu - \mu_{\text{id}}$ and the ideal gas chemical potential $\mu_{\text{id}} = k_B T \ln(\rho_b \Lambda^3)$. Here, $V_{\text{ext}}(\boldsymbol{r})$ is the external potential produced by the test particle as

$$V_{\text{ext}}(r) = \begin{cases} \infty, & r < \sigma, \\ u(r), & r \geq \sigma, \end{cases} \tag{53}$$

In this form, the radial distribution, defined as $g(\boldsymbol{r}) = \rho(\boldsymbol{r})/\rho_b$, can be obtained by

$$g(\boldsymbol{r}) = \exp\left[-\beta V_{\text{ext}}(\boldsymbol{r})\right] \exp\left[c^{(1)}_{\text{exc}}(\boldsymbol{r},[\rho]) + \beta\mu_{\text{exc}}\right], \tag{54}$$

such that, in the low-density limit $g(\boldsymbol{r}) \sim e^{-\beta V_{\text{ext}}(\boldsymbol{r})}$.

Further, the equilibrium condition, Eq. (52), is solved numerically, minimizing the grand potential using the FIRE algorithm. The initial density profile is set as $\rho(r) = \rho_b g_{\text{hs}}(r;\rho_b)$. The radial geometry is spatially discretized with a grid spacing of 0.01σ and radius 5σ, which characterizes the cutoff radius. The algorithm convergence criterion is $\max\{|\delta\Omega[\{\rho\}]/\delta\rho(r)|\} \leq \texttt{atol} = 10^{-7}$.

In Fig. 7, the predicted radial distribution functions of hard-sphere fluids for different densities are compared with MC simulation data available in the literature [62]. The figure shows the magnificent performance of the FMT to describe the structure of $g(r)$ as well as its contact value $g(\sigma)$.

The radial distribution functions for the YK fluid are presented in Fig. 8. On the scales of the figures, the different DFT formulations predict the MC data [63] admirably. The likelihood of each DFT formulation is around 40% to represent the MC data. This result reaffirms the fact that both DFT formulations can be used to calculate the radial distribution function of YK fluids.

The radial distribution functions for the SW fluid are presented in Fig. 9. On the scales of the figures, the different DFT formulations indeed predict the MC data [26,64]. The likelihood of each DFT formulation is around 94% to represent the MC data. This result reaffirms that both DFT formulations can be used to calculate the radial distribution function of SW fluids. Although, we can see a little strange structure introduced by the MFT term on the MMFT results.

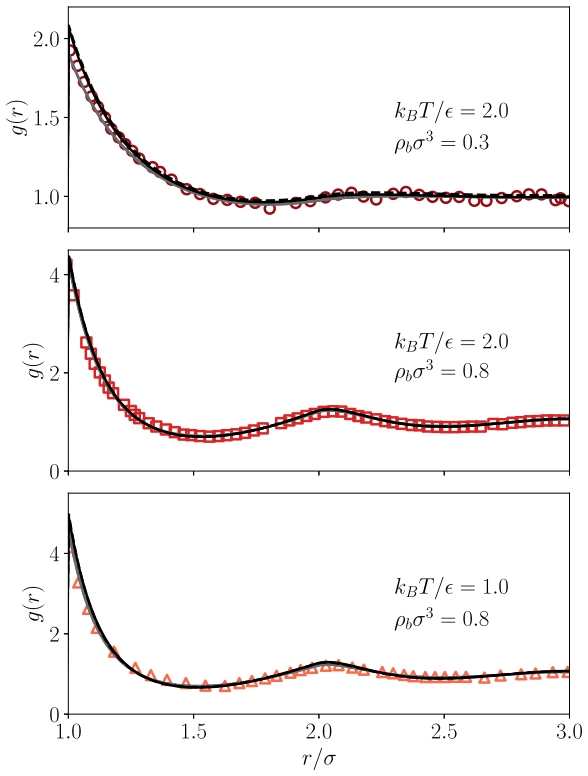

Fig. 8. Radial distribution function for an attractive Yukawa fluid with $\lambda\sigma = 1.8$ at reduced temperature $k_BT/\epsilon = 2.0$ and two different reduced densities. Open symbols: MC data from Ref. [63]. Dashed grey line: MWDA-BH. Solid grey line: MWDA-SCPT. Dashed black line: MMFT-BH. Solid black line: MMFT-SCPT. The profile of $\rho\sigma^3 = 0.8$ is shifted upward by 1.0.

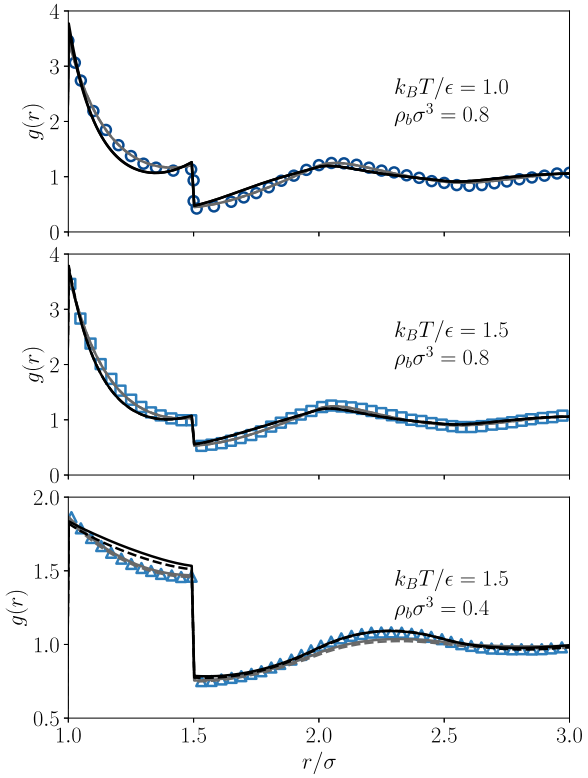

Fig. 9. Radial distribution function for a square-well fluid with $\lambda\sigma = 1.5$ and two different reduced density and two different reduced temperatures. Open symbols: MC data from Ref. [26,64]. Dashed grey line: MWDA-BH. Solid grey line: MWDA-SCPT. Dashed black line: MMFT-BH. Solid black line: MMFT-SCPT. The profile of $k_BT/\epsilon = 1.5$ is shifted upward by 1.0.

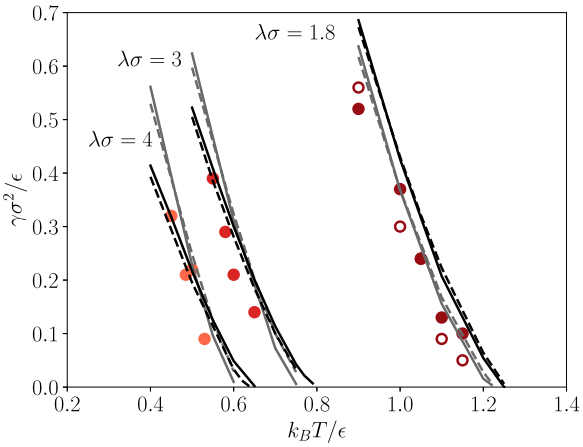

Fig. 10. Surface tension, γ, at the vapor/liquid interface of an attractive Yukawa fluid as a function of reduced temperatures k_BT/ϵ. Open and closed symbols: MC and MD data from Ref. [65], respectively. Dashed grey line: MWDA-BH. Solid grey line: MWDA-SCPT. Dashed black line: MMFT-BH. Solid black line: MMFT-SCPT.

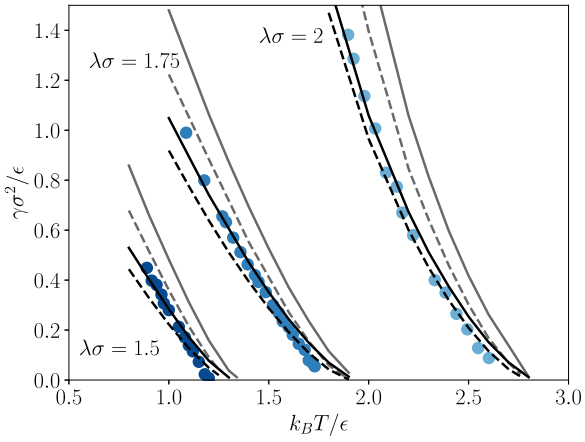

Fig. 11. Surface tension, γ, at the vapor/liquid interface of an attractive square-well fluid as a function of reduced temperatures k_BT/ϵ. Closed symbols: MD data from Ref. [60]. Dashed grey line: MWDA-BH. Solid grey line: MWDA-SCPT. Dashed black line: MMFT-BH. Solid black line: MMFT-SCPT.

These results confirm that the radial distribution function results are not sensitive to variations in the DFT formulation.

3.4. Vapor-liquid coexistence

To describe a planar vapor-liquid interface, we also solve a planar density profile $\rho(z)$ from the condition given by Eq. (49). The interface is spatially discretized in 1000 grid points covering a width of 20σ, leading to a grid spacing of 0.02σ. The numerical procedure is the same as discussed in Section 3.2. The main difference here is the initial density profile, which is defined by symmetrical form,

$$\rho(z) = \frac{1}{2}(\rho_l + \rho_v) - \frac{1}{2}(\rho_l - \rho_v)\tanh(\frac{2z}{\delta}), \tag{55}$$

where $z = 0$ is the position of the interface, ρ_l and ρ_v are the liquid and vapor densities, respectively, and δ is the width of the interfacial region. The coexistence densities for a given T are determined on the same geometry to avoid numerical errors. The δ is determined by minimizing the grand potential as a unique function of that parameter. Further, the grand potential is minimized using the FIRE algorithm for the density profile $\rho(z)$ with the convergence criterion given by $\max\{|\delta\Omega[\{\rho\}]/\delta\rho(r)|\} \leq \texttt{atol} = 10^{-5}$. This unconstrained minimization, in opposition to the Eq. (55), is necessary to allow oscillation on the density profile that appear mainly at low temperatures.

The surface tension of the system is calculated by the difference of the grand potential of the interface and that of the bulk phases. Once we have the interfacial density profile calculated by the DFT, the surface tension γ can be calculated from

$$\gamma = \frac{\Omega[\rho(z)]}{A} + \int_{-\infty}^{\infty} p\mathrm{d}z\,, \tag{56}$$

where A is the cross-sectional area of the system, and p is the bulk pressure of the fluid related to the bulk grand-potential by $p = -\Omega_b/V$.

In Fig. 10, the surface tension results for the attractive YK fluids with a range of $\lambda\sigma = 1.8$, 3.0, and 4.0 are presented. At low temperatures, the MMFT results are quantitatively more consistent with the MD simulation data [65] than the MWDA results. As we can see in Table 3, the likelihoods of the MMFT results predict the MD data are greater than the likelihoods of the MWDA results. The MMFT-BH results are 4% more likely to represent the MD data than the MMFT-SCPT results, but it seems to be not statistically relevant. To better discriminate models, we would need MD data at lower temperatures.

The surface tension results for the attractive SW fluid with range of $\lambda\sigma = 1.5$, 1.75, and 2.0 are presented in Fig. 11. The MMFT-SCPT results predict the MD simulation data [60] wonderfully well. The likelihood to describe the MD data for the MMFT-SCPT is 11% greater than the likelihood of MMFT-BH, as shown in Table 3.

Therefore, both MMFT-BH and MMFT-SCPT can be used to predict the surface tension for YK and SW fluid.

4. Conclusions

We developed a self-consistent perturbation theory based on the coupling parameter expansion but using the radial distribution function $g(r)$ calculated by DFT. Unlike the conventional DFT formulations, an advantage of this theory is that there is no need to solve the OZ equation for the direct correlation function. Therefore, this perturbation theory can be applied to any pair potential. When compared to the second-order Barker-Henderson perturbation theory, the self-consistent theory predicts better coexistence liquid density and saturation pressure for both YK and SW fluids. The critical temperature and pressure are overestimated on both perturbation theories. We understand that our results are not renormalized, and a renormalization group analysis should be done in future works.

To use our self-consistent perturbative DFT, we presented two different versions of the perturbative contribution to the excess Helmholtz free-energy: one based in a modified WDA (MWDA); and another based on a modified MFT (MMFT). These two functional forms are evaluated and compared with MC data of liquid-wall interaction, radial distribution function, and liquid-vapor interface for YK and SW fluids. For the YK fluid, the MWDA is better than MMFT for the BH perturbation theory representing an increase of 7% on the likelihood to describe the set of MC/MD data. However, MMFT is better than MWDA when it comes to SCPT, with an increase of 10% on the likelihood. For SW fluids, the MMFT is always better than the MWDA either for BH or SCPT, increasing 10% and 48% on the likelihood, respectively. Moreover, both DFT formulations can generate the radial distribution functions needed by the SCPT.

In this work, we define a likelihood to compare the DFT models with the MC or MD data. However, most of the available MC data have no uncertainties reported. Our normalization of the residual sum of squares χ^2 was used to define a scale for the data. So,

some care must be taken to compare likelihood to different MC data. For this reason, the likelihood values for different sets of MC data should not be compared to each other. As an example, the likelihood for the SW $g(r)$ cannot be compared to the YK $g(r)$. But the likelihood for the SW $g(r)$ calculated with MWDA-BH can be compared to the likelihood for the SW $g(r)$ calculated with MMFT-SCPT because the MC data are the same.

Computationally, the MWDA and MMFT versions are equivalent in performance and easiness of implementation. Here, we must emphasize here that these versions of DFT are attempts to describe the exact structures of the hard-core fluids described at the level of perturbation theory. There is no exact solution as a fundamental measure theory for the perturbative contribution of the excess free-energy.

Finally, we would like to mention possible extensions of the presented self-consistent perturbative DFT. The SCPT can be extended to treat soft-core fluids, associating fluids and solids. Moreover, it would be of interest to generalize the SCPT to describe mixtures and chain fluids.

The data availability

The data that support the findings of this study are available from the corresponding author upon reasonable request.

Declaration of Competing Interest

The authors declare that they have no known competing financial interests or personal relationships that could have appeared to influence the work reported in this paper.

CRediT authorship contribution statement

Elvis do A. Soares: Methodology, Formal analysis, Writing - original draft. **Amaro G. Barreto Jr.:** Conceptualization, Supervision, Writing - review & editing. **Frederico W. Tavares:** Supervision, Conceptualization, Methodology, Writing - review & editing.

Acknowledgments

The authors thank the financial support from the Brazilian National Agency of Petroleum, Natural Gas and Biofuels (ANP, Brazil) and PETROBRAS through the Clause of Investments in Research, Development and Innovation. This study was also partially financed by the National Council for Technological and Scientific Development (CNPq, Brazil) and the Coordination for the Improvement of Higher Education Personnel (CAPES, Brazil).

Appendix A. The weighted densities on different geometries

The weighted densities necessary to the DFT calculations must be calculated differently in each geometry. On the symmetrical 1D planar geometry, the convolution must be calculated as follows. First, let remember that in 1D planar geometry, the density can be written as $\rho(\boldsymbol{r}) = \rho(z)$, and its Fourier Transform is

$$\widetilde{\rho}(\boldsymbol{k}) = \int \mathrm{d}\boldsymbol{r}\, \rho(\boldsymbol{r}) e^{i\boldsymbol{k}\cdot\boldsymbol{r}} = \widetilde{\rho}(k_z)(2\pi)^2\delta(k_x)\delta(k_y) \tag{A.1}$$

where the two Dirac-delta functions are present due to the homogeneity of the density field on the $x-y$ plane. Now, let evaluate the weighted density $n(\boldsymbol{r})$ through the convolution theorem

$$n(\boldsymbol{r}) = \int \mathrm{d}\boldsymbol{r}'\, \rho(\boldsymbol{r}')\omega(\boldsymbol{r}-\boldsymbol{r}') = \int \frac{\mathrm{d}\boldsymbol{k}}{(2\pi)^3}\widetilde{\rho}(\boldsymbol{k})\widetilde{\omega}(\boldsymbol{k})e^{-i\boldsymbol{k}\cdot\boldsymbol{r}} \tag{A.2}$$

and using the Eq. (A.1), we get

$$n(\boldsymbol{r}) = \frac{1}{2\pi}\int \mathrm{d}k_z\, \widetilde{\rho}(k_z)\widetilde{\omega}(k_z)e^{-ik_z z} \tag{A.3}$$

where $\widetilde{\omega}(k_z) = \widetilde{\omega}(k_x = 0, k_y = 0, k_z)$. Returning to the real space, we finally obtain

$$n^{(\mathrm{planar})}(z) = \int_{-\infty}^{\infty} \mathrm{d}z'\, \rho(z')\omega^{(\mathrm{planar})}(z-z'). \tag{A.4}$$

For the 1D spherically symmetric geometry, the density can be written as $\rho(\boldsymbol{r}) = \rho(r)$, and its Fourier Transform is

$$\widetilde{\rho}(\boldsymbol{k}) = \int \mathrm{d}\boldsymbol{r}\, \rho(\boldsymbol{r})e^{i\boldsymbol{k}\cdot\boldsymbol{r}} = 4\pi\int \mathrm{d}r\, r^2\rho(r)j_0(kr) \tag{A.5}$$

where j_ℓ is the spherical Bessel function of ℓ-order. Let remember the identity

$$e^{i\boldsymbol{k}\cdot\boldsymbol{r}} = 4\pi\sum_{\ell=0}^{\infty}\sum_{m=-\ell}^{\ell} i^\ell j_\ell(kr)Y_{\ell m}(\theta,\phi)Y^*_{\ell m}(\theta_k,\phi_k) \tag{A.6}$$

where $Y_{\ell m}$ are the spherical harmonic functions. Now, let evaluate the weighted density $n(\boldsymbol{r})$ through the convolution theorem, Eq. (A.2), and applying the indentity given by the Eq. (A.6) we get

$$n(\boldsymbol{r}) = \frac{2}{\pi}\int_0^\infty \mathrm{d}r'\, r'^2\rho(r')\int_0^\infty \mathrm{d}k\, k^2\widetilde{\omega}(k)j_0(kr)j_0(kr'), \tag{A.7}$$

where we used of the symmetry $\widetilde{\omega}(\boldsymbol{k}) = \widetilde{\omega}(k)$ and the othornormality of $Y_{\ell m}$. The integral on k is a little tricky but can be solved using the definition of the spherical Bessel function, such that

$$\begin{aligned}&\frac{2}{\pi}\int_0^\infty \mathrm{d}k\, k^2\widetilde{\omega}(k)j_0(kr)j_0(kr')\\ &= \frac{1}{rr'}\frac{1}{2\pi}\int \mathrm{d}k\,\widetilde{\omega}(k)e^{ik(r-r')} = \frac{1}{rr'}\omega(r-r')\end{aligned} \tag{A.8}$$

and the 1D spherical convolution must be calculated by

$$n^{(\mathrm{spher})}(r) = \frac{1}{r}\int_0^\infty \mathrm{d}r'\, r'\rho(r')\omega^{(\mathrm{spher})}(r-r'). \tag{A.9}$$

In both geometries, the weight functions can be obtained by a 1D inverse Fourier Transform of the 3D Fourier Transform of the original weight function, in the form

$$\omega^{(1\mathrm{D})}(z) = \int \frac{\mathrm{d}k}{2\pi}\widetilde{\omega}(k)e^{-ikr} \tag{A.10}$$

As an example, the spherical 3D Fourier transform of the $\omega_3(r)$ from the FMT is

$$\begin{aligned}\widetilde{\omega}_3(k) &= \int \omega_3(r)\frac{\sin kr}{kr}4\pi r^2\mathrm{d}r\\ &= \frac{\pi\sigma^2}{k}\left[\frac{\sin(k\sigma/2)}{(k\sigma/2)^2} - \frac{\cos(k\sigma/2)}{k\sigma/2}\right],\end{aligned} \tag{A.11}$$

and the inverse planar 1D Fourier Transform is given by

$$\begin{aligned}\omega_3^{(\mathrm{planar})}(z) &= \frac{1}{2\pi}\int \tilde{\omega}_3(k)e^{-ikz}\mathrm{d}k\\ &= \pi[(\sigma/2)^2 - z^2]\Theta(\sigma/2-|z|),\end{aligned} \tag{A.12}$$

such that the 1D convolution must be obtained by Eq. (A.4). Thus, we can calculate the others 1D planar weight functions with the same method. The other linearly independent planar 1D weight function are $\omega_2^{(\mathrm{planar})}(z) = \pi\sigma\Theta(\sigma/2-|z|)$ and $\boldsymbol{\omega}_{v2}^{(\mathrm{planar})}(z) = 2\pi z\Theta(\sigma/2-|z|)\hat{\boldsymbol{z}}$. For the 1D spherical geometry, the weight functions are the same, changing $z \to r$. However, we are not interested in the inner region ($r < \sigma$) of the hard-sphere contact, such that we start the convolution integral at $r = \sigma$.

For the WDA weight function, the process is similar to the $\omega_3(r)$ weight function from the FMT. In fact, the planar 1D weight function is $\omega_{\mathrm{wda}}^{(\mathrm{planar})}(z) = \frac{3}{4(\psi\sigma)^3}[(\psi\sigma)^2 - z^2]\Theta(\psi\sigma-|z|)$.

All the convolutions and the FMT functional on planar and spherical geometries are implemented in a Python code by our group, i.e., the Eq. (A.4) and Eq. (A.9) were solved using the *convolve1d* function from *Numpy package* [66].

Appendix B. The pair interaction potential on different geometries

As discussed in Appendix A, the convolutions involving the pair potential $u(r)$ and the density $\rho(\boldsymbol{r})$ must also be defined in the 1D geometries. We known that the convolutions are necessary to calculate the terms of our modified mean-field theory as

$$F_{\text{mmft}}[\rho(\boldsymbol{r})] = \frac{1}{2}\int \mathrm{d}\boldsymbol{r} \int \mathrm{d}\boldsymbol{r}'\, \rho(\boldsymbol{r})\rho(\boldsymbol{r}')u(\boldsymbol{r}-\boldsymbol{r}') = \frac{1}{2}\int \mathrm{d}\boldsymbol{r}\, \rho(\boldsymbol{r})\Psi(\boldsymbol{r}) \tag{B.1}$$

where $\Psi(\boldsymbol{r}) = \int \mathrm{d}\boldsymbol{r}'\, \rho(\boldsymbol{r}')u(\boldsymbol{r}-\boldsymbol{r}')$ is the potential convolution. Let start with the Yukawa (YK) potential, Eq. (43), whose the Fourier Transform is

$$\begin{aligned}\widetilde{u}_{\text{YK}}(k) &= \int u_{\text{YK}}(r)\frac{\sin kr}{kr}4\pi r^2\mathrm{d}r \\ &= -\frac{4\pi\epsilon\sigma^3}{(k\sigma)^2+(\lambda\sigma)^2}\left[\cos(k\sigma)+\lambda\sigma\frac{\sin(k\sigma)}{k\sigma}\right] \\ &\quad + \frac{4\pi\epsilon\sigma^2}{k}\left[\frac{\cos(k\sigma)}{k\sigma}-\frac{\sin(k\sigma)}{(k\sigma)^2}\right],\end{aligned} \tag{B.2}$$

which in the limit of very small hard-core region returns to the well-known result of $\lim_{\sigma\to 0}\widetilde{u}_{\text{YK}}(k) = 4\pi\epsilon\sigma/(k^2+\lambda^2)$. The inverse 1D Fourier Transform gives the 1D planar YK potential written as

$$u_{\text{YK}}^{(1\text{D})}(z) = \begin{cases} -\epsilon\pi\left(\frac{\sigma(2+\lambda\sigma)}{\lambda}-z^2\right), & |z|<\sigma, \\ -2\pi\epsilon\frac{e^{-\lambda(|z|-\sigma)}}{\lambda/\sigma}, & |z|\geq\sigma \end{cases} \tag{B.3}$$

Once more, the 1D planar convolution must be calculated by Eq. (A.4) and the 1D spherical convolution by Eq. (A.9), as discussed in Appendix A.

Similarly, the Square-Well (SW) potential, Eq. (44), has as Fourier Transform

$$\begin{aligned}\widetilde{u}_{\text{SW}}(k) &= \int u_{\text{SW}}(r)\frac{\sin kr}{kr}4\pi r^2\mathrm{d}r \\ &= \frac{4\pi\epsilon(\lambda\sigma)^2}{k}\left[\frac{\cos(k\lambda\sigma)}{k\lambda\sigma}-\frac{\sin(k\lambda\sigma)}{(k\lambda\sigma)^2}\right],\end{aligned} \tag{B.4}$$

and the 1D inverse Fourier Transform gives the 1D planar SW potential in the form $u_{\text{SW}}^{(1\text{D})}(z) = -\epsilon\pi(\lambda^2\sigma^2 - z^2)\Theta(\lambda\sigma - |z|)$.

Appendix C. The interpolation of the perturbation free-energy

Hermite splines are typically used for interpolation of numeric data specified at some values $x_1, x_2, \ldots, x_n$, to obtain a smooth continuous function. The data should consist of the desired function value and derivatives at each x_i. The Hermite formula is applied to each interval $[x_i, x_{i+1}]$ independently, being defined by

$$H_3(x) = a_0 + a_1x + a_2x^2 + a_3x^3, \tag{C.1}$$

with the following constraints of the original function values $f(x_i)$ and its derivatives at the borders of the interval as

$$H_3(x_i) = f_i, \quad H_3(x_{i+1}) = f_{i+1}, \quad H_3'(x_i) = \left.\frac{\mathrm{d}f}{\mathrm{d}x}\right|_i, \quad H_3'(x_{i+1}) = \left.\frac{\mathrm{d}f}{\mathrm{d}x}\right|_{i+1}, \tag{C.2}$$

which are necessary to determine the coefficients a_i. The two polynomials resulting from these constraints are the cubic Hermite basis functions, given in the form Davis [67]

$$h_0(z) = 1 - 3z^2 + 2z^3, \tag{C.3a}$$

$$h_1(z) = z - 2z^2 + z^3, \tag{C.3b}$$

and the interpolating cubic Hermite polynomial can be written as

$$H_3(x) = f_ih_0(\widetilde{x}) + f_{i+1}h_0(1-\widetilde{x}) + \left.\frac{\mathrm{d}f}{\mathrm{d}x}\right|_i \Delta x_i h_1(\widetilde{x}) - \left.\frac{\mathrm{d}f}{\mathrm{d}x}\right|_{i+1}\Delta x_i h_1(1-\widetilde{x}). \tag{C.4}$$

where $\widetilde{x} = (x - x_i)/\Delta x_i$ and $\Delta x_i = x_{i+1} - x_i$.

This cubic Hermite function was used to interpolate the Helmholtz free-energy per particle f given by the first-order terms of the perturbation theories, Eqs. (21) or (25), as a function of the reduced density $\rho\sigma^3$. The range of the 1D table on the reduced density was chosen to be $\rho\sigma^3 = [0;1]$ with $\Delta\rho\sigma^3 = 0.02$. Increasing the precision of the table to $\Delta\rho\sigma^3 = 0.01$ does not result in improvements. The first derivatives necessary to construct the interpolant function are calculated from a centered difference approximation with second-order accuracy on the table values. On the border of the table, we use a forward/backward finite difference approximation again with second-order accuracy.

The one-dimensional cubic Hermite spline can be extended to 2D by interpolating each parcel of the Eq. (C.4) again on the second dimension.

$$\begin{aligned}H_3(x,y) = {} & f_{i,j}h_0(\tilde{x})h_0(\tilde{y}) + f_{i+1,j}h_0(1-\tilde{x})h_0(\tilde{y}) \\ & + f_{i,j+1}h_0(\tilde{x})h_0(1-\tilde{y}) + f_{i+1,j+1}h_0(1-\tilde{x})h_0(1-\tilde{y}) \\ & + \left.\frac{\partial f}{\partial x}\right|_{i,j}\Delta x_i h_1(\tilde{x})h_0(\tilde{y}) - \left.\frac{\partial f}{\partial x}\right|_{i+1,j}\Delta x_i h_1(1-\tilde{x})h_0(\tilde{y}) \\ & + \left.\frac{\partial f}{\partial x}\right|_{i,j+1}\Delta x_i h_1(\tilde{x})h_0(1-\tilde{y}) - \left.\frac{\partial f}{\partial x}\right|_{i+1,j+1}\Delta x_i h_1(1-\tilde{x})h_0(1-\tilde{y}) \\ & + \left.\frac{\partial f}{\partial y}\right|_{i,j}\Delta y_i h_0(\tilde{x})h_1(\tilde{y}) - \left.\frac{\partial f}{\partial y}\right|_{i+1,j}\Delta y_i h_0(1-\tilde{x})h_1(\tilde{y}) \\ & + \left.\frac{\partial f}{\partial y}\right|_{i,j+1}\Delta y_i h_0(\tilde{x})h_1(1-\tilde{y}) - \left.\frac{\partial f}{\partial y}\right|_{i+1,j+1}\Delta y_i h_0(1-\tilde{x})h_1(1-\tilde{y}) \\ & + \left.\frac{\partial^2 f}{\partial x\partial y}\right|_{i,j}\Delta x_i\Delta y_i h_1(\tilde{x})h_1(\tilde{y}) - \left.\frac{\partial^2 f}{\partial x\partial y}\right|_{i+1,j}\Delta x_i\Delta y_i h_1(1-\tilde{x})h_1(\tilde{y}) \\ & - \left.\frac{\partial^2 f}{\partial x\partial y}\right|_{i,j+1}\Delta x_i\Delta y_i h_1(\tilde{x})h_1(1-\tilde{y}) + \left.\frac{\partial^2 f}{\partial x\partial y}\right|_{i+1,j+1}\Delta x_i\Delta y_i h_1(1-\tilde{x})h_1(1-\tilde{y})\end{aligned} \tag{C.5}$$

where $\widetilde{y} = (y - y_i)/\Delta y_i$ and $\Delta y_i = y_{i+1} - y_i$.

This bi-cubic Hermite function was used to interpolate the Helmholtz free-energy per particle f given by the second-order terms of the perturbation theories, Eqs. (22) or (26), as a function of the reduced density $\rho\sigma^3$ and reduced temperature k_BT/ϵ. The 2D range of the table was chosen to be $\rho\sigma^3 = [0;1]$ with $\Delta\rho\sigma^3 = 0.02$ and $k_BT/\epsilon = [0;4]$ with $\Delta k_BT/\epsilon = 0.02$ in those reduced units. This range of 50 points in density and 50 points in

temperature is large enough for our DFT calculations of inhomogeneous fluids. Refining the table does not increase the precision of the table and does not result in any improvement. Again, the first and second-mixed derivatives necessary to construct the interpolant function are calculated from a centered difference approximation with second-order accuracy on the table values. We use a forward/backward finite difference approximation with second-order accuracy on the border of the table

In return to this nontrivial investment, the values of the function, first partial derivatives, and second partial derivatives are reproduced exactly at the grid points, changing continuously as the interpolating point moves from one grid cell to the next. Using Eq. (C.5) as the interpolating function, the Helmholtz free-energy per particle is given by a bi-cubic polynomial. Because the first law of thermodynamics is given by

$$\mathrm{d}f = -s\mathrm{d}T + \frac{p}{\rho^2}\mathrm{d}\rho\,, \tag{C.6}$$

where s is the entropy per particle and p is the pressure. Bi-quadratic polynomials gives the pressure and entropy per particle. All the derivatives of these thermodynamic quantities are given by bi-linear interpolations. In particular, the mixed derivative,

$$\frac{\partial^2 f}{\partial T \partial \rho} = -\left.\frac{\partial s}{\partial \rho}\right|_T = \frac{1}{\rho^2}\left.\frac{\partial p}{\partial T}\right|_\rho , \tag{C.7}$$

represents the Maxwell thermodynamic relation that is satisfied on the whole interpolation range. Therefore, the mixed derivative $\partial^2 f/\partial T\partial\rho$ is extremely necessary to make the free-energy thermodynamically consistent. Lastly, note that the partial derivatives of bi-cubic interpolant are determined by the derivatives of the two basis functions given by Eq. (C.3).

References

[1] R. Evans, Density functional theory for inhomogeneous fluids I: simple fluids in equilibrium, Lectures at 3rd Warsaw School of Statistical Physics, Kazimierz Dolny, 2009. (June 27)

[2] R. Evans, M. Oettel, R. Roth, G. Kahl, et al., New developments in classical density functional theory, J. Phys. 28 (24) (2016) 240401, doi:10.1088/0953-8984/28/24/240401.

[3] Y. Rosenfeld, Free-energy model for the inhomogeneous hard-sphere fluid mixture and density-functional theory of freezing, Phys. Rev. Lett. 63 (9) (1989) 980–983, doi:10.1103/PhysRevLett.63.980.

[4] R. Roth, Fundamental measure theory for hard-sphere mixtures: a review, J. Phys. 22 (6) (2010) 063102, doi:10.1088/0953-8984/22/6/063102. URL http://stacks.iop.org/0953-8984/22/i=6/a=063102?key=crossref.e8ded4d3b4b40a58361c21e1fbb1abc0

[5] M.B. Sweatman, Weighted density functional theory for simple fluids: supercritical adsorption of a Lennard-Jones fluid in an ideal slit pore, Phys. Rev. E 63 (3) (2001) 031102, doi:10.1103/PhysRevE.63.031102.

[6] Z. Tang, L.E. Scriven, H.T. Davis, Density-functional perturbation theory of inhomogeneous simple fluids, J. Chem. Phys. 95 (4) (1991) 2659–2668, doi:10.1063/1.460918.

[7] N. Choudhury, S.K. Ghosh, Density functional theory of ordering in charge-stabilized colloidal dispersions, Phys. Rev. E (1995), doi:10.1103/PhysRevE.51.4503.

[8] F.-Q. You, Y.-X. Yu, G.-H. Gao, Structure of inhomogeneous attractive and repulsive hard-core Yukawa fluid: grand canonical Monte Carlo simulation and density functional theory study, J. Phys. Chem. B 109 (8) (2005) 3512–3518, doi:10.1021/jp045112h.

[9] B. Peng, Y.-X. Yu, A Density functional theory with a mean-field weight function: applications to surface tension, adsorption, and phase transition of a Lennard-Jones fluid in a slit-like pore, J. Phys. Chem. B 112 (48) (2008) 15407–15416, doi:10.1021/jp805697p.

[10] P. Tarazona, Free-energy density functional for hard spheres, Phys. Rev. A 31 (4) (1985) 2672–2679, doi:10.1103/PhysRevA.31.2672.

[11] Y. Rosenfeld, M. Schmidt, H. Löwen, P. Tarazona, et al., Fundamental-measure free-energy density functional for hard spheres: dimensional crossover and freezing, Phys. Rev. E 55 (4) (1997) 4245–4263, doi:10.1103/PhysRevE.55.4245.

[12] Y.X. Yu, J. Wu, Structures of hard-sphere fluids from a modified fundamental-measure theory, J. Chem. Phys. 117 (22) (2002) 10156–10164, doi:10.1063/1.1520530.

[13] S. Zhou, Perturbation density functional theory for density profile of a nonuniform and uniform hard core attractive Yukawa model fluid, J. Phys. Chem. B 106 (31) (2002) 7674–7680, doi:10.1021/jp020431z.

[14] Z. Shi-Qi, Mean spherical approximation-based partitioned density functional theory, Commun. Theor. Phys. 40 (6) (2003) 721–726, doi:10.1088/0253-6102/40/6/721.

[15] Z. Jin, Y. Tang, J. Wu, A perturbative density functional theory for square-well fluids, J. Chem. Phys. 134 (17) (2011) 174702, doi:10.1063/1.3585677.

[16] T. Bernet, M.M. Piñeiro, F. Plantier, C. Miqueu, et al., Generalization of the fundamental-measure theory beyond hard potentials: the square-well fluid case, J. Phys. Chem. C 121 (11) (2017) 6184–6190, doi:10.1021/acs.jpcc.7b00797.

[17] T. Bernet, M.M. Piñeiro, F. Plantier, C. Miqueu, et al., Effect of structural considerations on the development of free energy functionals for the square-well fluid, Mol. Phys. 116 (15–16) (2018) 1977–1989, doi:10.1080/00268976.2018.1438677.

[18] Z. Ye, H. Chen, J. Cai, H. Liu, Y. Hu, et al., Density functional theory of homopolymer mixtures confined in a slit, J. Chem. Phys. 125 (12) (2006) 124705, doi:10.1063/1.2354087.

[19] Y. Liu, H. Liu, Y. Hu, J. Jiang, et al., Density functional theory for adsorption of gas mixtures in metal-organic frameworks, J. Phys. Chem. B 114 (8) (2010) 2820–2827, doi:10.1021/jp9104932.

[20] G. Shen, X. Ji, X. Lu, A hybrid perturbed-chain SAFT density functional theory for representing fluid behavior in nanopores, J. Chem. Phys. 138 (22) (2013) 224706, doi:10.1063/1.4808160.

[21] G. Shen, X. Lu, X. Ji, Modeling of molecular gas adsorption isotherms on porous materials with hybrid PC-SAFT-DFT, Fluid Phase Equilib. 382 (2014) 116–126, doi:10.1016/j.fluid.2014.09.002.

[22] E. Sauer, J. Gross, Classical density functional theory for liquid-fluid interfaces and confined systems: a functional for the perturbed-chain polar statistical associating fluid theory equation of state, Ind. Eng. Chem. Res. 56 (14) (2017) 4119–4135, doi:10.1021/acs.iecr.6b04551.

[23] E.L. Camacho Vergara, G.M. Kontogeorgis, X. Liang, Gas adsorption and interfacial tension with classical density functional theory, Ind. Eng. Chem. Res. 58 (14) (2019) 5650–5664, doi:10.1021/acs.iecr.9b00137.

[24] V.M. Sermoud, G.D. Barbosa, A.G. Barreto, F.W. Tavares, et al., Quenched solid density functional theory coupled with PC-SAFT for the adsorption modeling on nanopores, Fluid Phase Equilib. 521 (2020) 112700, doi:10.1016/j.fluid.2020.112700. URL https://linkinghub.elsevier.com/retrieve/pii/S0378381220302466

[25] J. Eller, J. Gross, Free-energy-averaged potentials for adsorption in heterogeneous slit pores using PC-SAFT classical density functional theory, Langmuir (2021), doi:10.1021/acs.langmuir.0c03287.

[26] J. Largo, J.R. Solana, S.B. Yuste, A. Santos, et al., Pair correlation function of short-ranged square-well fluids, J. Chem. Phys. 122 (8) (2005) 084510, doi:10.1063/1.1855312.

[27] I. Guillén-Escamilla, E. Schöll-Paschinger, R. Castañeda Priego, A parametrisation of the direct correlation function for the square-shoulder fluid, Mol. Phys. 108 (2) (2010) 141–150, doi:10.1080/00268970903539592.

[28] M. Khanpour, R. Hashim, Pair correlation function from the Barker-Henderson perturbation theory of fluids: the structure of square-well and square-shoulder potentials, Phys. Chem. Liq. 51 (2) (2013) 203–217, doi:10.1080/00319104.2012.717894.

[29] T.W. Cochran, Y.C. Chiew, Thermodynamic and structural properties of repulsive hard-core Yukawa fluid: integral equation theory, perturbation theory and Monte Carlo simulations, J. Chem. Phys. 121 (3) (2004) 1480–1486, doi:10.1063/1.1759616.

[30] E.B. El Mendoub, J.-F. Wax, N. Jakse, Evolution of the liquid-vapor coexistence of the hard-core Yukawa fluid as a function of the interaction range, J. Chem. Phys. 132 (16) (2010) 164503, doi:10.1063/1.3385894.

[31] P. Orea, C. Tapia-Medina, D. Pini, A. Reiner, et al., Thermodynamic properties of short-range attractive Yukawa fluid: simulation and theory, J. Chem. Phys. 132 (11) (2010) 114108, doi:10.1063/1.3357352.

[32] M. Heinen, P. Holmqvist, A.J. Banchio, G. Ngele, et al., Pair structure of the hard-sphere Yukawa fluid: an improved analytic method versus simulations, Rogers-Young scheme, and experiment, J. Chem. Phys. 134 (4) (2011), doi:10.1063/1.3524309.

[33] W.A. Curtin, N.W. Ashcroft, Weighted-density-functional theory of inhomogeneous liquids and the freezing transition, Phys. Rev. A 32 (5) (1985) 2909–2919, doi:10.1103/PhysRevA.32.2909.

[34] R.D. Groot, N.M. Faber, J.P. van der Eerden, Hard sphere fluids near a hard wall and a hard cylinder, Mol. Phys. 62 (4) (1987) 861–871, doi:10.1080/00268978700102631.

[35] A.R. Denton, N.W. Ashcroft, Modified weighted-density-functional theory of nonuniform classical liquids, Phys. Rev. A 39 (9) (1989) 4701–4708, doi:10.1103/PhysRevA.39.4701.

[36] J.A. Barker, D. Henderson, Perturbation theory and equation of state for fluids: the square-well potential, J. Chem. Phys. 47 (8) (1967) 2856–2861, doi:10.1063/1.1712308.

[37] J.A. Barker, D. Henderson, Perturbation theory and equation of state for fluids. II. A successful theory of liquids, J. Chem. Phys. 47 (11) (1967) 4714–4721, doi:10.1063/1.1701689.

[38] F.W. Tavares, J.M. Prausnitz, Analytic calculation of phase diagrams for solutions containing colloids or globular proteins, Colloid Polym. Sci. 282 (6) (2004) 620–632, doi:10.1007/s00396-003-0987-x.

[39] S. Zhou, Thermodynamic perturbation theory in fluid statistical mechanics, Phys. Rev. E 74 (3) (2006) 031119, doi:10.1103/PhysRevE.74.031119.

[40] S. Zhou, J.R. Solana, Comprehensive investigation about the second order term of thermodynamic perturbation expansion, J. Chem. Phys. 131 (13) (2009) 134106, doi:10.1063/1.3242801.

[41] S. Zhou, Fifth-order thermodynamic perturbation theory of uniform and nonuniform fluids, Phys. Rev. E 77 (4) (2008) 041110, doi:10.1103/PhysRevE.77.041110.
[42] R. Evans, Density functionals in the theory of nonuniform fluids, in: D. Henderson (Ed.), Fundamentals of Inhomogeneous Fluids, CRC Press, 1992, pp. 85–175.
[43] R. Roth, R. Evans, A. Lang, G. Kahl, et al., Fundamental measure theory for hard-sphere mixtures revisited: the White Bear version, J. Phys. 14 (46) (2002) 12063–12078, doi:10.1088/0953-8984/14/46/313.
[44] G.A. Mansoori, N.F. Carnahan, K.E. Starling, T.W. Leland, et al., Equilibrium thermodynamic properties of the mixture of hard spheres, J. Chem. Phys. 54 (4) (1971) 1523–1525, doi:10.1063/1.1675048.
[45] N.F. Carnahan, K.E. Starling, Equation of state for nonattracting rigid spheres, J. Chem. Phys. 51 (2) (1969) 635–636, doi:10.1063/1.1672048.
[46] T. Boublík, I. Nezbeda, K. Hlavatỳ, Statistical Thermodynamics of Simple Liquids and Their Mixtures, Elsevier, 1980.
[47] S. Zhou, Improvement on macroscopic compressibility approximation and beyond, J. Chem. Phys. 125 (14) (2006) 144518, doi:10.1063/1.2353834.
[48] R. Leidl, H. Wagner, Hybrid WDA: a weighted-density approximation for inhomogeneous fluids, J. Chem. Phys. 98 (5) (1993) 4142–4148, doi:10.1063/1.465022.
[49] M. Johnson, S. Nordholm, Generalized van der Waals theory. VI. Application to adsorption, J. Chem. Phys. 75 (4) (1981) 1953–1957, doi:10.1063/1.442220.
[50] Y.-X. Yu, A novel weighted density functional theory for adsorption, fluid-solid interfacial tension, and disjoining properties of simple liquid films on planar solid surfaces, J. Chem. Phys. 131 (2) (2009) 024704, doi:10.1063/1.3174928.
[51] J.F. Lutsko, Density functional theory of inhomogeneous liquids. I. The liquid-vapor interface in Lennard-Jones fluids, J. Chem. Phys. 127 (5) (2007) 054701, doi:10.1063/1.2753500.
[52] S. Zhou, J.R. Solana, Excellence of numerical differentiation method in calculating the coefficients of high temperature series expansion of the free energy and convergence problem of the expansion, J. Chem. Phys. 141 (24) (2014) 244506, doi:10.1063/1.4904881.
[53] P. Gregory, Bayesian Logical Data Analysis for the Physical Sciences: A Comparative Approach with Mathematica® Support, Cambridge University Press, 2005.
[54] T.J. Archdeacon, Correlation and Regression Analysis: A Historian's Guide, Univ of Wisconsin Press, 1994.
[55] E. Bitzek, P. Koskinen, F. Gähler, M. Moseler, P. Gumbsch, et al., Structural relaxation made simple, Phys. Rev. Lett. 97 (17) (2006) 1–4, doi:10.1103/PhysRevLett.97.170201.
[56] J. Guénolé, W.G. Nöhring, A. Vaid, F. Houllé, Z. Xie, A. Prakash, E. Bitzek, et al., Assessment and optimization of the fast inertial relaxation engine (fire) for energy minimization in atomistic simulations and its implementation in lammps, Comput. Mater. Sci. 175 (2020) 109584, doi:10.1016/j.commatsci.2020.109584. URL https://linkinghub.elsevier.com/retrieve/pii/S0927025620300756
[57] E.d. A. Soares, PyFIRE, 2020, (https://github.com/elvissoares/PyFIRE).
[58] V.M. Sermoud, G.D. Barbosa, E.A. Soares, A.G. Barreto, F.W. Tavares, et al., Exploring the multiple solutions of the classical density functional theory using metadynamics based method, unpublished (2021).
[59] J.K. Singh, Surface tension and vapour-liquid phase coexistence of variable-range hard-core attractive Yukawa fluids, Mol. Simul. 35 (10–11) (2009) 880–887, doi:10.1080/08927020902787796.
[60] J.K. Singh, D.A. Kofke, J.R. Errington, Surface tension and vapor-liquid phase coexistence of the square-well fluid, J. Chem. Phys. 119 (6) (2003) 3405–3412, doi:10.1063/1.1590313.
[61] J.R. Henderson, F. van Swol, Grand potential densities of wall-liquid interfaces approaching complete drying, J. Chem. Phys. 89 (8) (1988) 5010–5014, doi:10.1063/1.455644.
[62] J.A. Barker, D. Henderson, Monte Carlo values for the radial distribution function of a system of fluid hard spheres, Mol. Phys. 21 (1) (1971) 187–191, doi:10.1080/00268977100101331.
[63] K.P. Shukla, Phase equilibria and thermodynamic properties of hard core Yukawa fluids of variable range from simulations and an analytical theory, J. Chem. Phys. 112 (23) (2000) 10358–10367, doi:10.1063/1.481673.
[64] A. Lang, G. Kahl, C.N. Likos, H. Löwen, M. Watzlawek, et al., Structure and thermodynamics of square-well and square-shoulder fluids, J. Phys. 11 (50) (1999) 10143–10161, doi:10.1088/0953-8984/11/50/308.
[65] M. González-Melchor, A. Trokhymchuk, J. Alejandre, Surface tension at the vapor/liquid interface in an attractive hard-core Yukawa fluid, J. Chem. Phys. 115 (8) (2001) 3862–3872, doi:10.1063/1.1384553.
[66] C.R. Harris, K.J. Millman, S.J. van der Walt, R. Gommers, P. Virtanen, D. Cournapeau, E. Wieser, J. Taylor, S. Berg, N.J. Smith, R. Kern, M. Picus, S. Hoyer, M.H. van Kerkwijk, M. Brett, A. Haldane, J.F. del R'ıo, M. Wiebe, P. Peterson, P. G'erard-Marchant, K. Sheppard, T. Reddy, W. Weckesser, H. Abbasi, C. Gohlke, T.E. Oliphant, Array programming with NumPy, Nature 585 (7825) (2020) 357–362, doi:10.1038/s41586-020-2649-2.
[67] P.J. Davis, Interpolation and Approximation, Courier Corporation, 1975.